NASA TECHNICAL NOTE

NASA TN D-3932

NASA TN D-3932

EFFECTS OF REYNOLDS NUMBER AND FLOW INCIDENCE ON THE FORCE CHARACTERISTICS OF A FAMILY OF FLAT-FRONT CYLINDERS

by Vernard E. Lockwood

Langley Research Center
Langley Station, Hampton, Va.

NATIONAL AERONAUTICS AND SPACE ADMINISTRATION • WASHINGTON, D. C. • MAY 1967

NASA TN D-3932

EFFECTS OF REYNOLDS NUMBER AND FLOW INCIDENCE ON THE FORCE CHARACTERISTICS OF A FAMILY OF FLAT-FRONT CYLINDERS

By Vernard E. Lockwood

Langley Research Center
Langley Station, Hampton, Va.

NATIONAL AERONAUTICS AND SPACE ADMINISTRATION

For sale by the Clearinghouse for Federal Scientific and Technical Information
Springfield, Virginia 22151 – CFSTI price $3.00

EFFECTS OF REYNOLDS NUMBER AND FLOW INCIDENCE ON THE FORCE CHARACTERISTICS OF A FAMILY OF FLAT-FRONT CYLINDERS

By Vernard E. Lockwood
Langley Research Center

SUMMARY

The cross-flow characteristics of three flat-front two-dimensional cylinders have been determined for a range of Reynolds numbers from 0.12×10^6 to 1.60×10^6. The data showed a large effect of Reynolds number, flow incidence, and cylinder breadth on the cross-flow characteristics. As the Reynolds number was increased from 0.12×10^6, all three cylinders were characterized by sudden increases in the side-force coefficient which resulted in positive values for an incidence-angle range from about 5^o to 120^o. A comparison of these data with the data from previous investigations indicated that the range of Reynolds numbers over which the large positive values of the side force existed were dependent on cylinder breadth, with the broader cylinder having the larger range of positive side forces.

INTRODUCTION

The current interest in large supersonic commercial transport aircraft has focused attention on the aerodynamic influence of the fuselage forebody because the relative length of the forebody of these aircraft is considerably greater than that of their subsonic counterparts. Of particular interest is the effect of the fuselage forebody on directional stability. Reference 1 illustrates the importance of forebody cross-sectional shape on the directional stability at moderate and high angles of attack for a supersonic transport configuration. These results indicate that a rather modest departure from a circular cross section results in sizable increases in directional stability at moderate and high angles of attack. Previous investigations of two-dimensional cylinders of various cross sections (such as those of refs. 2 and 3) have shown the sensitivity of the viscous cross flow to Reynolds number and flow incidence and have indicated cross sections which might offer increased directional stability to three-dimensional configurations at angles of attack. One such cross section, illustrated in figure 14 of reference 3 and which is similar to that used on the model of reference 1 (although broader), showed the desirable positive cross-flow component for a wide range of Reynolds numbers.

As a result of the previous studies, an investigation of two-dimensional cylinders was made to provide basic data for the nose cross section of reference 1 and also to provide data on the effect of systematic variations in cross-sectional shape on the development of favorable side forces. In addition to the effect of cross-sectional shape, the effects of Reynolds number and flow incidence angle on the cross-flow characteristics of the cylinders were determined. The results of this study, together with the results of references 2 and 3, provide data on a series of geometrically related cross sections. The investigation was made in the Langley 300-MPH 7- by 10-foot tunnel over a range of Reynolds numbers from about 0.12×10^6 to 1.60×10^6.

SYMBOLS

The aerodynamic data and angles of incidence are referenced to the axis system shown in figure 1. The aerodynamic coefficients and Reynolds numbers have been corrected for the effects of wind-tunnel walls by the method of reference 4.

b	maximum width of cylinder normal to flow at zero flow incidence, meters
c	maximum depth of cylinder parallel to flow at zero flow incidence, 0.2032 meter
c_x	section longitudinal-force coefficient, $\frac{\text{Longitudinal force per unit length}}{b\rho V^2/2}$
c_y	section side-force coefficient, $\frac{\text{Side force per unit length}}{b\rho V^2/2}$
C_p	pressure coefficient, $\frac{\text{Local static pressure - Free-stream static pressure}}{\rho V^2/2}$
R	Reynolds number based on c
s	surface distance measured from the plane of symmetry at zero incidence to a given point on cylinder, meters
V	free-stream velocity, meters/second
α	angle of attack of a body in three-dimensional flow, degrees
β	angle of sideslip of a body in three-dimensional flow, degrees

ρ free-stream air density, kilograms/meter^3

ϕ angle of incidence of two-dimensional cylinders, degrees

MODELS AND APPARATUS

The cross-sectional dimensions of the three cylinders used in this investigation are presented in figure 2. These three cylinders (A, B, and C), a circular cylinder (ref. 2), and a flat-front cylinder (cylinder E of ref. 3) form a family of related shapes with progressing flatness on the surface facing the wind at zero angle of incidence. (See fig. 3.) The cross section of cylinder B was identical to the fuselage-forebody cross section utilized in reference 1.

The cylinders of this investigation were constructed of mahogany and were lacquered to produce a smooth finish. The cylinders, which were approximately 2.13 meters long, spanned the vertical dimension of the test section of the Langley 300-MPH 7- by 10-foot tunnel in a manner similar to that shown in figure 2(b) of reference 2. End plates similar to those shown in reference 2 were attached to the cylinders to minimize the effect of leakage through the small gaps in the floor and ceiling that are required in the support of the model. The forces were measured by means of the mechnical balance system that surrounds the test section.

TESTS

The cylinders were tested at constant flow incidence angles from 0^o to 180^o (transition free) over a range of Reynolds numbers, based on the depth of the cylinders, from 0.12×10^6 to 1.60×10^6. The Reynolds number variations were obtained by increasing the tunnel velocity. Since the tunnel stagnation pressure is atmospheric, the velocity variation also corresponds to a Mach number variation from about 0.03 to 0.37. (At the highest Mach numbers obtained, it is possible that local sonic flow existed at some incidence angles on the cylinder; in which case, compressibility effects might appear in conjunction with the Reynolds number effects. However, if such effects exist, they are small.) Cylinder B was also tested at constant Reynolds number at varying incidence angles. In separated flows, different approaches to a given test condition can yield different results, as in the case of cylinder B. Some of the differences noted between the two approaches are discussed subsequently.

RESULTS AND DISCUSSION

Side Force

The basic data as a function of Reynolds number for cylinders A, B, and C are presented in figures 4, 5, and 6, respectively. Of particular significance from directional-stability considerations at high angles of attack is the side force in the range of incidence angles between $\phi = 10^{\circ}$ and $\phi = 30^{\circ}$. These angles are representative of those in the cross-flow plane which exist on a three-dimensional body for angles of attack varying from 9° to about 30° at a sideslip angle of 5°. (The two-dimensional cross-flow angle may be related to the three-dimensional flow angle as shown in reference 2 by the equation: $\tan \phi = \tan \beta / \sin \alpha$). For the range of incidence angles from 5° to 120° as the Reynolds number is increased from 0.12×10^6, the side-force coefficient c_y is characterized by sudden increases which result in values as great as 1.2 (figs. 4, 5, and 6). As the Reynolds number is further increased, a second critical region is generally encountered in which c_y decreases but remains more positive than the subcritical values. Note that positive values of c_y are generally in evidence for incidence angles from 5° to 60°.

A comparison of the values of c_y for the three cylinders of this investigation, the circular cylinder of reference 2, and cylinder E of reference 3 is given in figure 7 for $\phi = 10^{\circ}$ and $\phi = 30^{\circ}$. (Note that the circular cylinder has a cross-flow component $c_y = -c_x \sin \phi$.) Figure 7 indicates a pattern in the development of the positive values of c_y which are dependent on cylinder cross-sectional shape. In general, the first transition begins at a lower Reynolds number and the second transition is delayed until a higher Reynolds number for the cylinders with the greater breadth and smaller corner radii.

Flow Characteristics

From the side-force data shown in figures 4 to 7, it becomes apparent that the cylinders undergo a considerable change in the flow as the Reynolds number is increased. This flow phenomenon has been discussed in references 2 and 3 from the results of tuft studies and pressure distributions. These results are utilized to aid in understanding the side-force characteristics of the cylinders of this investigation. The potential-flow pressure distribution for a circular cylinder and the flat-front cylinder E of reference 3, as well as the pressure distribution of the circular cylinder of reference 5, is also utilized to aid in understanding the flow phenomenon.

The force characteristics at low Reynolds numbers ($R = 0.15 \times 10^6$) are shown in figure 7(a). At zero and low angles of incidence, it is probable that a laminar separation occurs on the forward surfaces similar to that which occurs on a circular cylinder (see fig. 4 of ref. 5), judging from the similarity in cross-sectional shape and similarity in

potential-flow pressure distributions (fig. 8). Pressure distributions associated with this type of flow on a circular cylinder indicate small suction pressures on the forward face compared with the higher Reynolds number data; hence, only a small side force is developed. An illustration of the probable flow-separation characteristics for the cylinders of this investigation, which is also similar to that shown in sketch 3 of reference 2, is indicated in sketch 1.

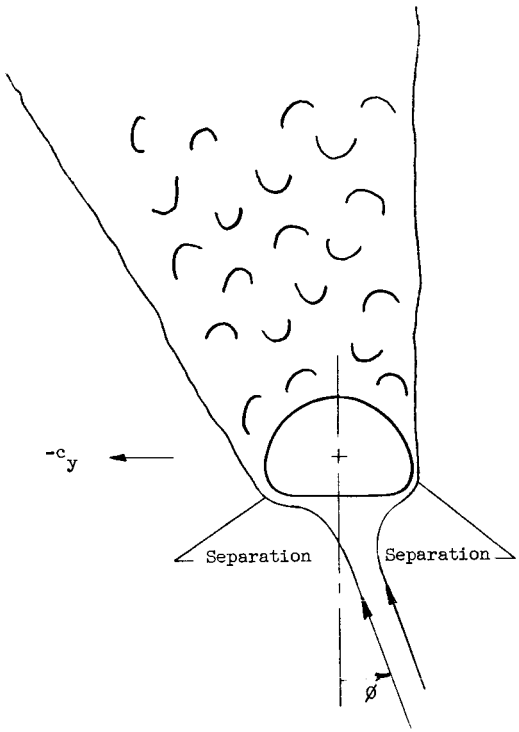

Sketch 1.- Separation on both forward surfaces.

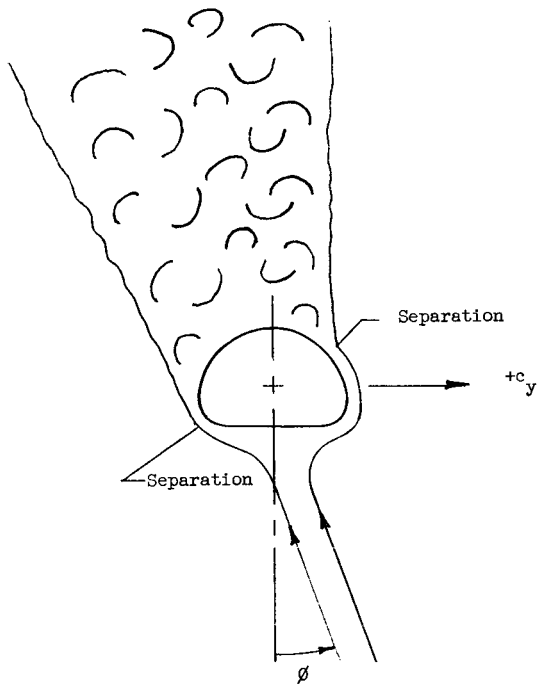

Sketch 2.- Separation on upper forward surface and lower rear surface.

The second flow regime is characterized by the development of a large positive side force c_y, such as that shown at $R = 0.4 \times 10^6$ in figures 7(a) and 7(c). The flow studies made in reference 2 indicate that the flow is attached on the lower surface well behind the maximum thickness point, as indicated in sketch 2. In this Reynolds number range, the upper surface probably has a separation on the forward face, although the decline in side force at some angles of incidence suggests that the separation point is moving rearward with increased Reynolds number. Eventually a Reynolds number is obtained in which the airflow contains enough energy to surmount the adverse pressure gradient of the upper

surface and the separation point moves rather abruptly to the rear, as shown in sketch 3. A reduction in wake is noted with a corresponding decrease in c_y. (A somewhat similar situation exists for the square cylinder of ref. 2.) The reduced values of c_y extend over a relatively large Reynolds number range as shown in figures 7(a) and 7(c). For cylinder A, little positive side force is developed for values of $R > 0.5 \times 10^6$.

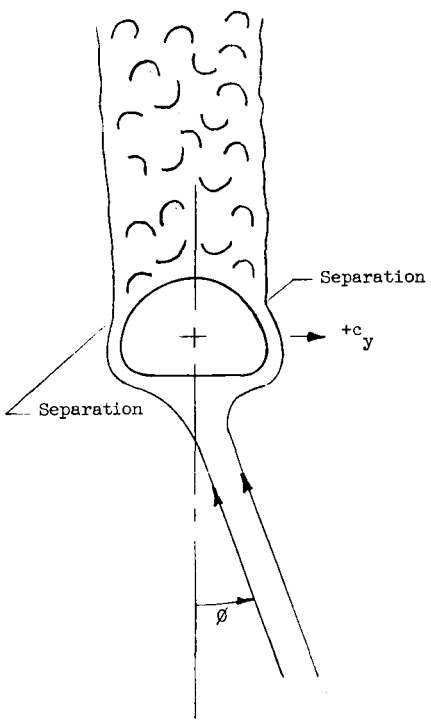

Sketch 3.- Separation on both rear surfaces.

Longitudinal Force

The longitudinal-force coefficients for cylinders A, B, and C are compared with those obtained for the circular cylinder of reference 2 and cylinder E of reference 3 for $\phi = 0^o$ (fig. 9). The data show no orderly variation in longitudinal-force coefficient with cylinder shape but, in general, the longitudinal-force coefficients for cylinders A, B, and C are greater than those for the circular cylinder of reference 2 and less than those for cylinder E of reference 3. The Reynolds numbers for complete transition lie between the value for the circular cylinder ($R \approx 0.4 \times 10^6$) and the value for cylinder E ($R \approx 0.62 \times 10^6$).

When the cylinders were reversed ($\phi = 180^o$), the values of c_x were about the same as those obtained for the circular cylinder of reference 2 for $R \approx 0.2 \times 10^6$. This characteristic might be expected since the cylinders are circular in cross section to the point of maximum thickness. Reynolds number transition characteristics of cylinders A and B at $\phi = 180^o$ appear to be about the same as those obtained at $\phi = 0^o$; cylinder C, however, because of its smaller corner radii has a wide transition range varying from $R \approx 0.25 \times 10^5$ to $R \approx 1.10 \times 10^6$ and has greater values of longitudinal-force coefficient.

The reversals of forces found in the side-force-coefficient data are also found in the longitudinal-force data for cylinder B. Data from figure 5 indicate positive values of c_x in the range of incidence angles between $\phi = 105^o$ and $\phi = 150^o$. However, the Reynolds number range for these conditions is limited, with values between $R \approx 0.3 \times 10^6$ and $R \approx 0.5 \times 10^6$.

Effect of Test Technique

In some investigations, different test techniques sometimes yield varying results, particularly when Reynolds number changes are significant. The data obtained on cylinder B is an example of some differences noted when the approach to a given operating condition was varied. Figure 10 compares results obtained by varying the angle of incidence while holding the Reynolds number constant with results obtained by varying the Reynolds number at constant angles of incidence. This comparison indicates a significant difference in values of c_x between $\phi = 60^o$ and $\phi = 135^o$ for the two methods of testing. The values of c_x obtained at constant angles of incidence were generally more positive. The values of c_y likewise show differences, although the variations tend to be of a more erratic nature. Some of the effects observed may be due to hysteresis resulting from variations in wind-tunnel velocity. An example of hysteresis for cylinder C is shown by the flagged symbols in figure 6(b). These flagged symbols indicate a transition Reynolds number having a value about 40 000 lower than the increasing Reynolds number.

CONCLUDING REMARKS

The results of an investigation of three flat-front two-dimensional cylinders showed a large effect of Reynolds number, flow incidence, and cylinder breadth on the cross-flow characteristics. As the Reynolds number was increased from 0.12×10^6, all three cylinders were characterized by sudden increases in the side-force coefficient which resulted in positive values for an incidence-angle range from about 5^o to 120^o. A comparison of these data with the data from previous investigations indicated that the range of Reynolds numbers over which the large positive values of the side force existed were dependent on cylinder breadth, with the broader cylinder having the larger range of positive side forces. The broader cylinders, in general, gave the larger values of longitudinal-force coefficients, as would be expected because of the smaller corner radii.

Langley Research Center,
National Aeronautics and Space Administration,
Langley Station, Hampton, Va., November 17, 1966,
126-13-01-64-23.

REFERENCES

1. Lockwood, Vernard E.: Low-Speed Wind-Tunnel Studies Relating to Pitch-Up on a Supersonic Transport Model With a High-Aspect-Ratio Variable-Sweep Wing. NASA TN D-3542, 1966.

2. Polhamus, Edward C.: Effect of Flow Incidence and Reynolds Number on Low-Speed Aerodynamic Characteristics of Several Noncircular Cylinders With Applications to Directional Stability and Spinning. NASA TR R-29, 1959. (Supersedes NACA TN 4176.)

3. Polhamus, Edward C.; Geller, Edward W.; and Grunwald, Kalman J.: Pressure and Force Characteristics of Noncircular Cylinders as Affected by Reynolds Number With a Method Included for Determining the Potential Flow About Arbitrary Shapes. NASA TR R-46, 1959.

4. Allen, H. Julian; and Vincenti, Walter G.: Wall Interference in a Two-Dimensional-Flow Wind Tunnel, With Consideration of the Effect of Compressibility. NACA Rept. 782, 1944. (Supersedes NACA WRA-63.)

5. Lockwood, Vernard E.; and McKinney, Linwood W.: Effect of Reynolds Number on the Force and Pressure Distribution Characteristics of a Two-Dimensional Lifting Circular Cylinder. NASA TN D-455, 1960.

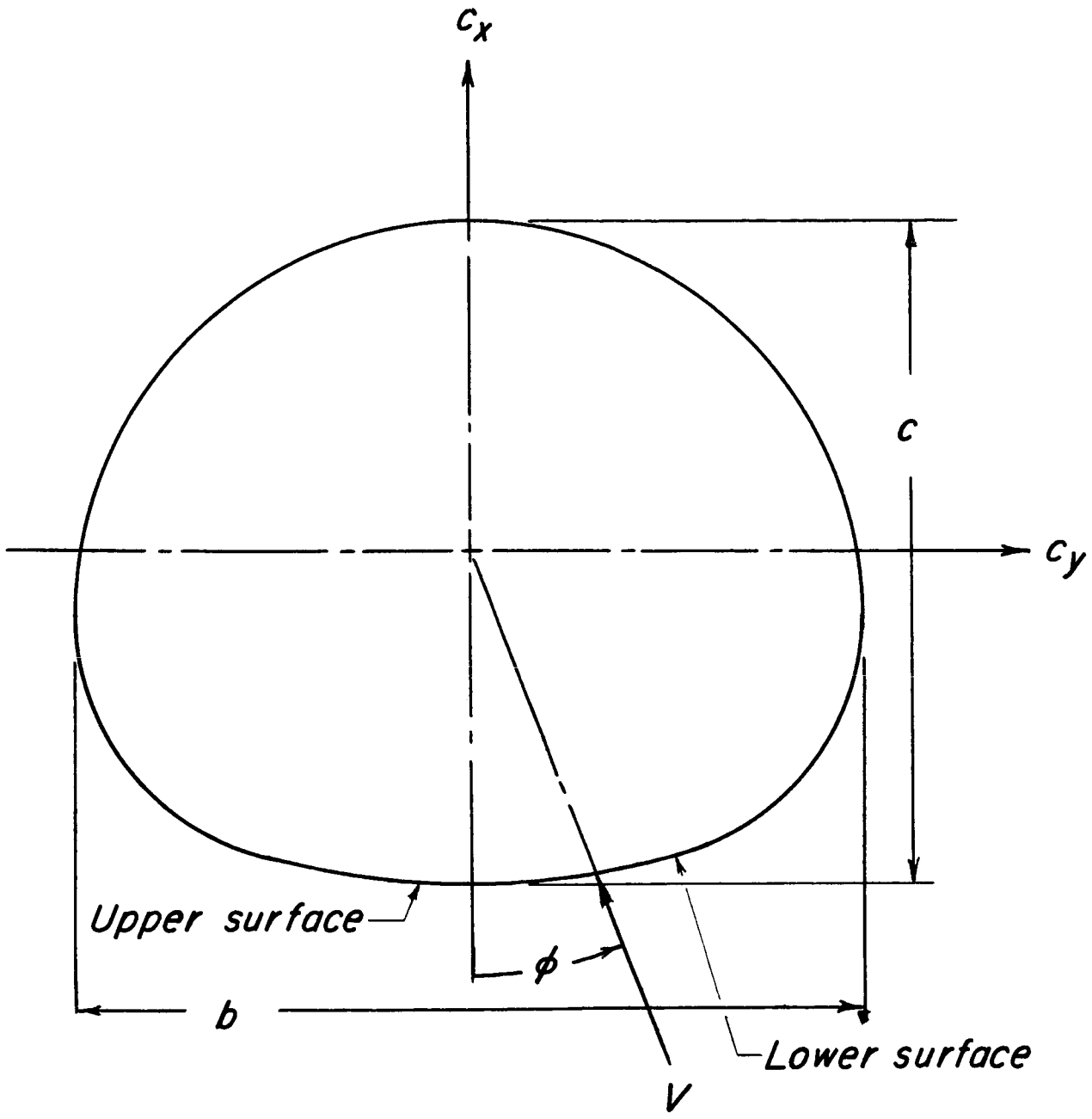

Figure 1.- Convention used to define positive sense of flow incidence, cylinder reference dimensions, and aerodynamic coefficients.

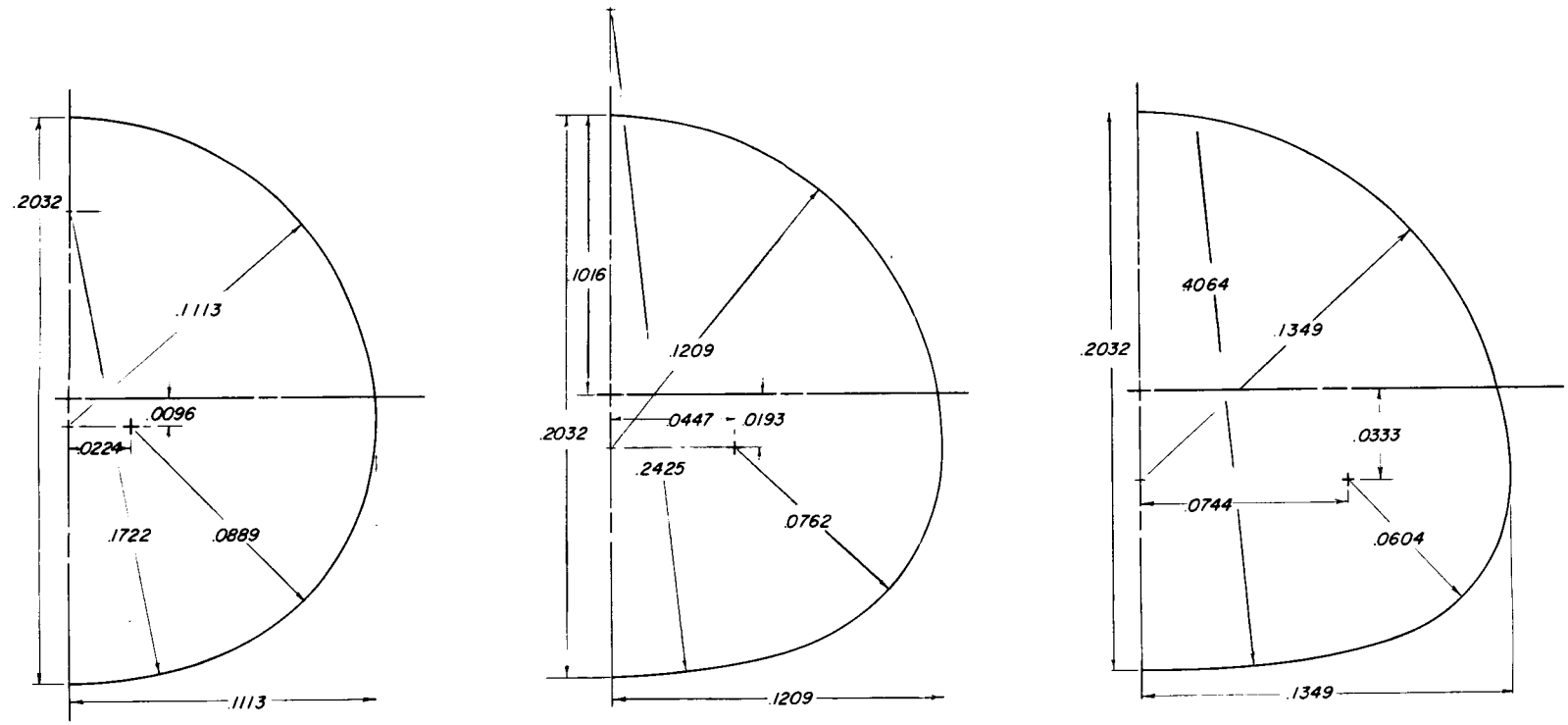

(a) Cylinder A.

(b) Cylinder B.

(c) Cylinder C.

Figure 2.- Sketch of the cross sections of two-dimensional cylinders tested at various flow incidences. Linear dimensions are given in meters.

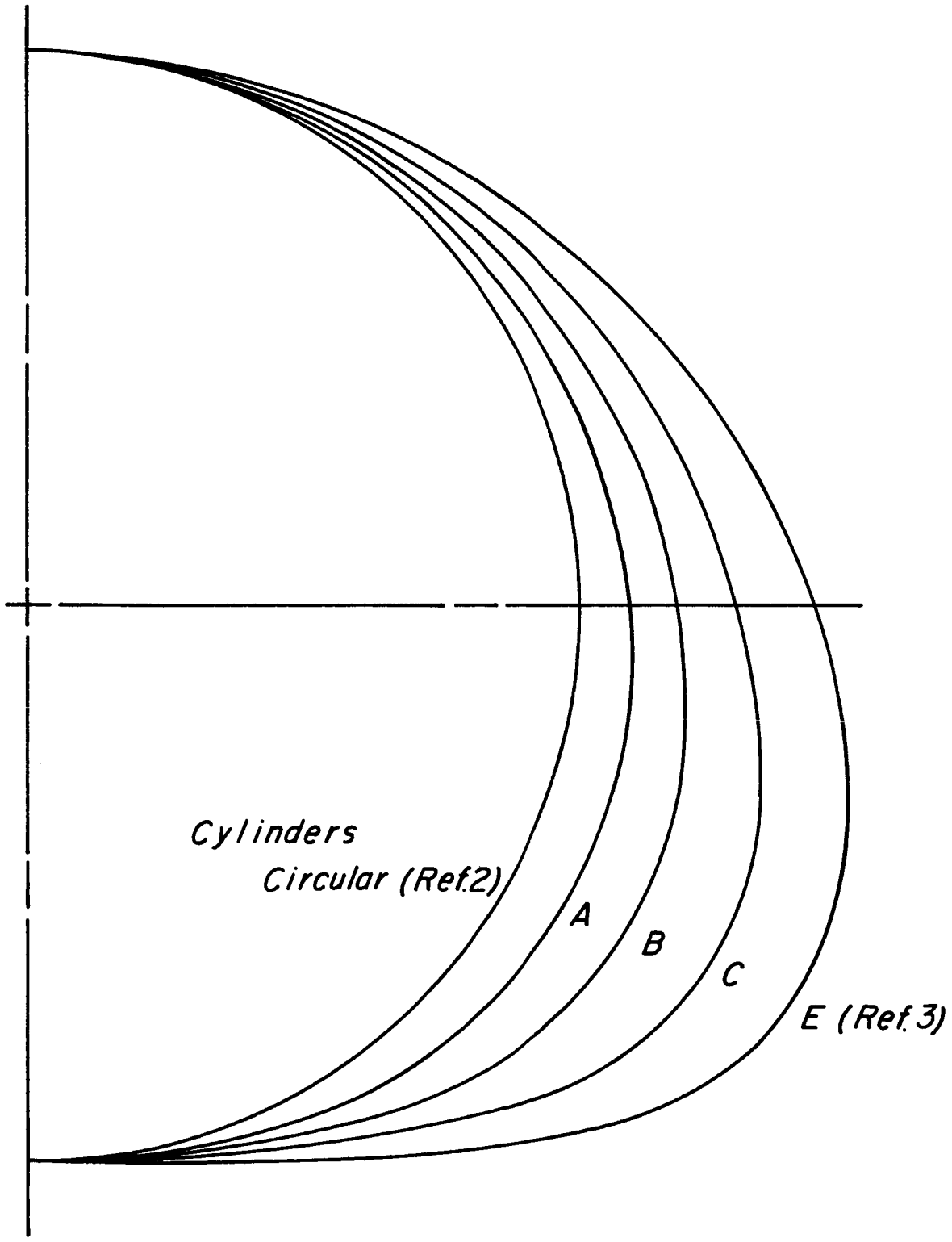

Figure 3.- Comparison of cylinder cross sections.

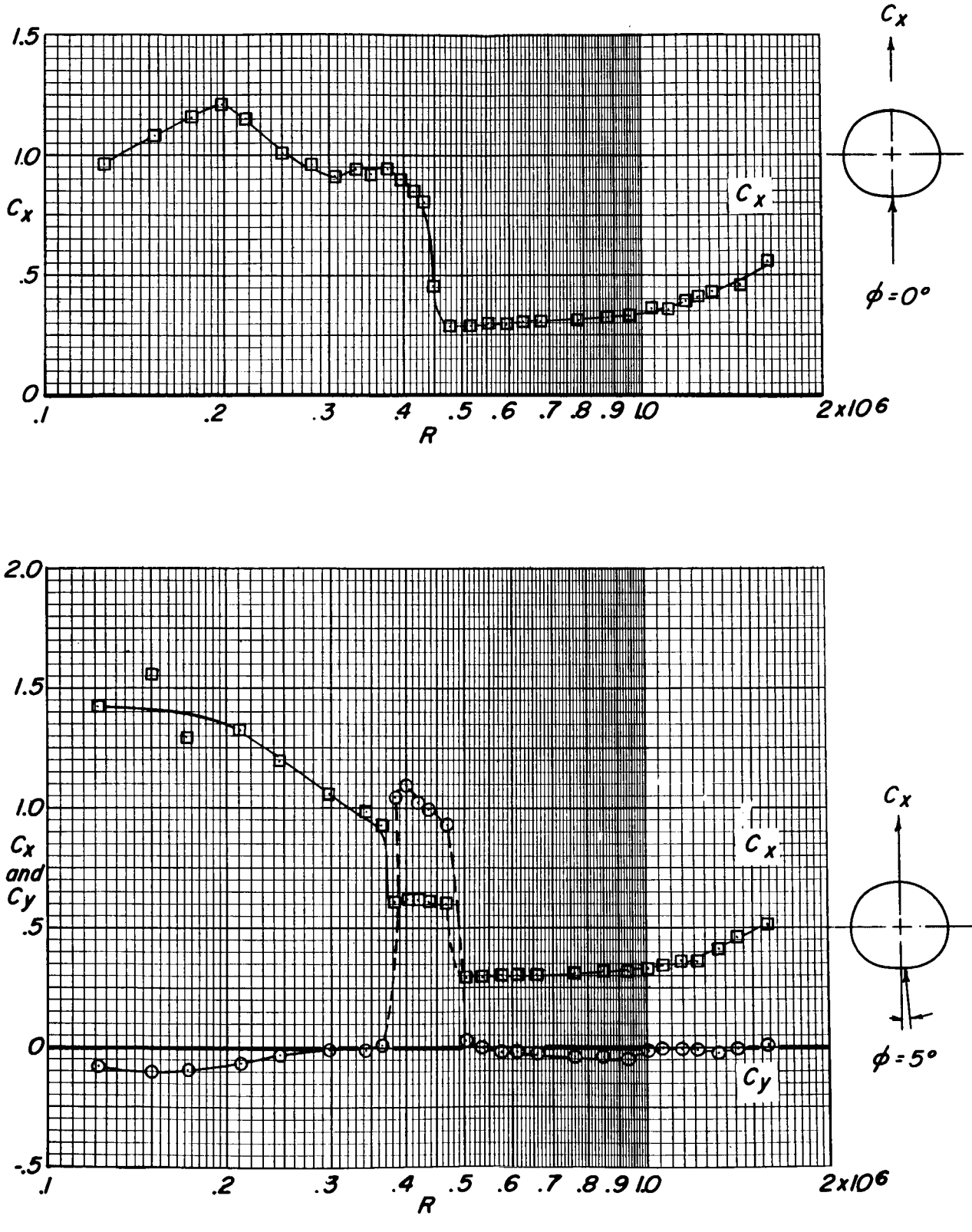

(a) $\Phi = 0^0$ and 5^0.

Figure 4.- Effect of Reynolds number at constant flow incidence on the force characteristics of cylinder A.

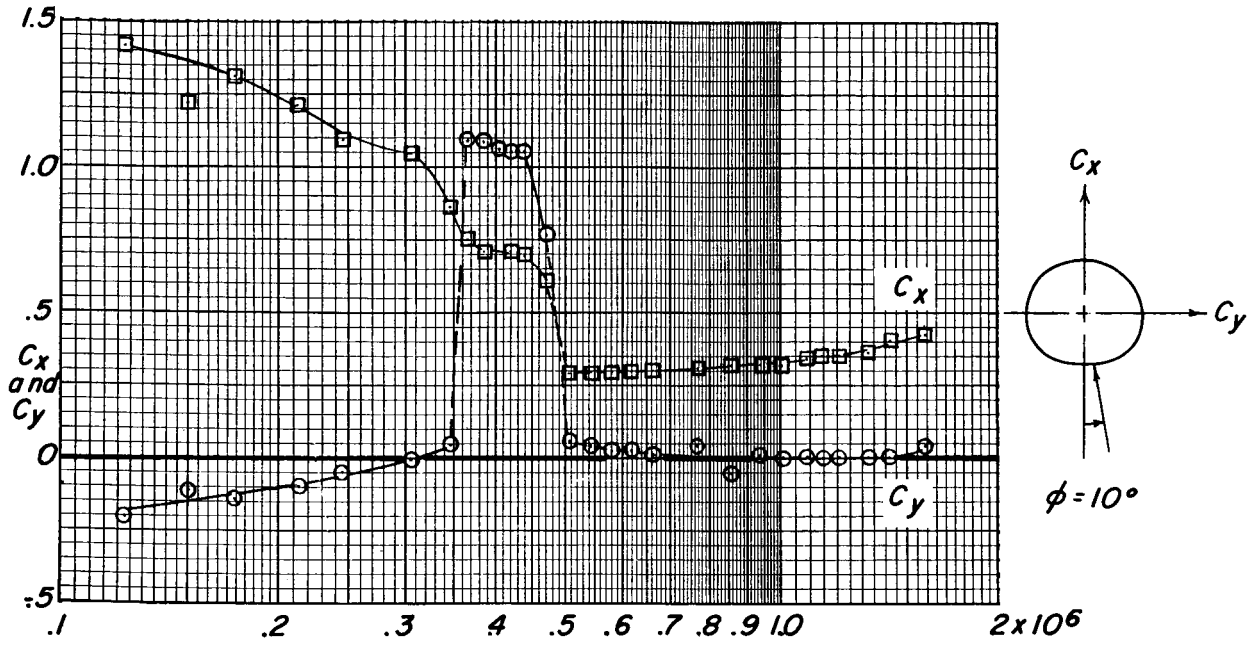

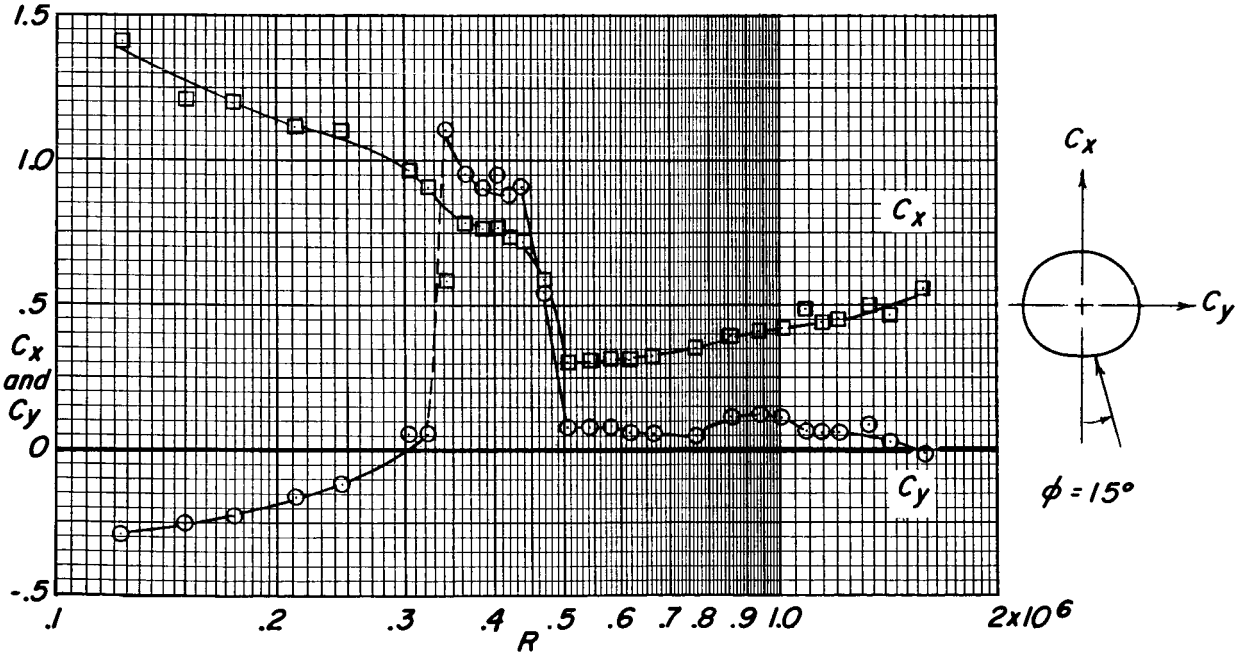

(b) $\Phi = 10^0$ and 15^0.

Figure 4.- Continued.

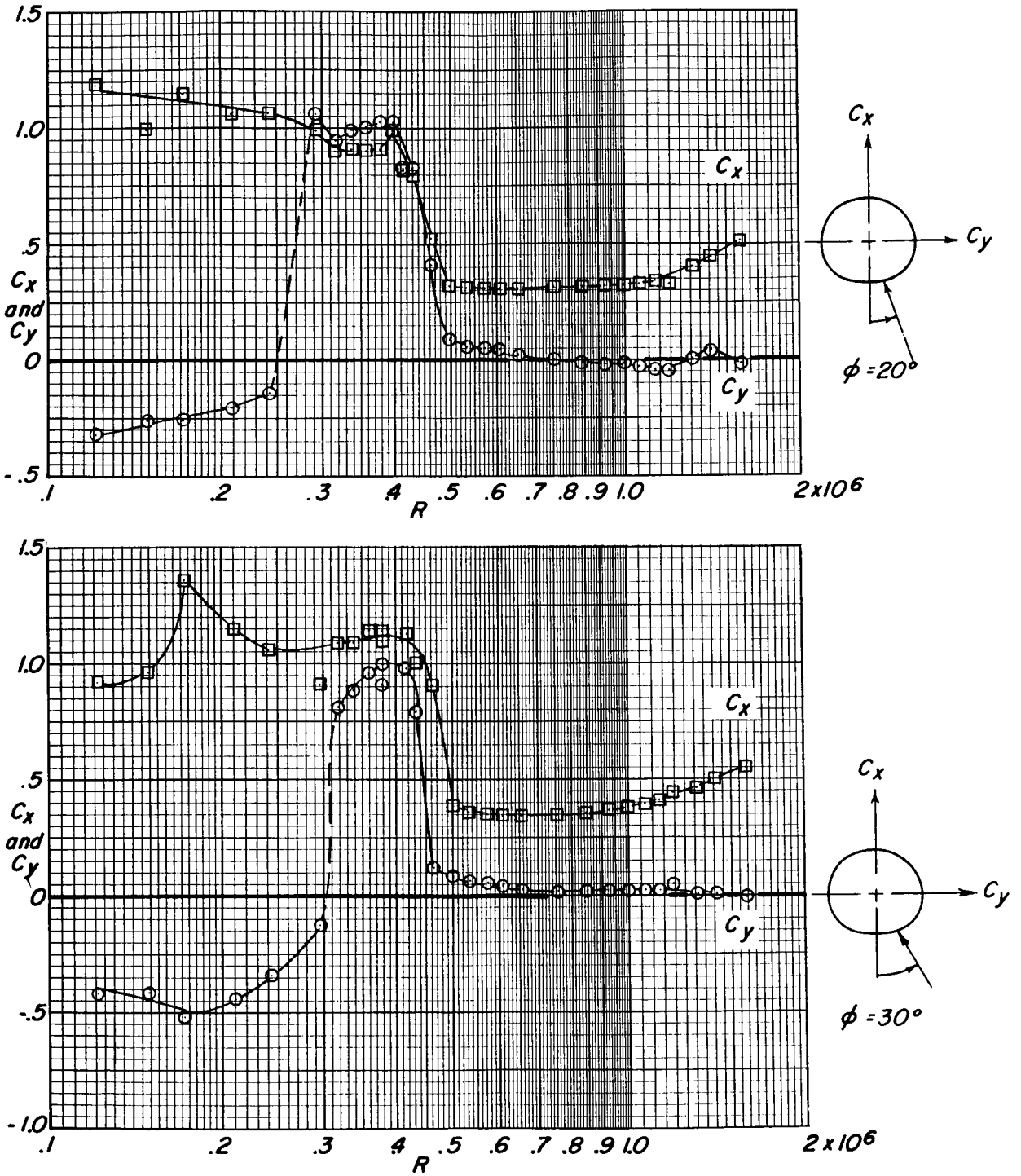

(c) $\Phi = 20^0$ and 30^0.

Figure 4.- Continued.

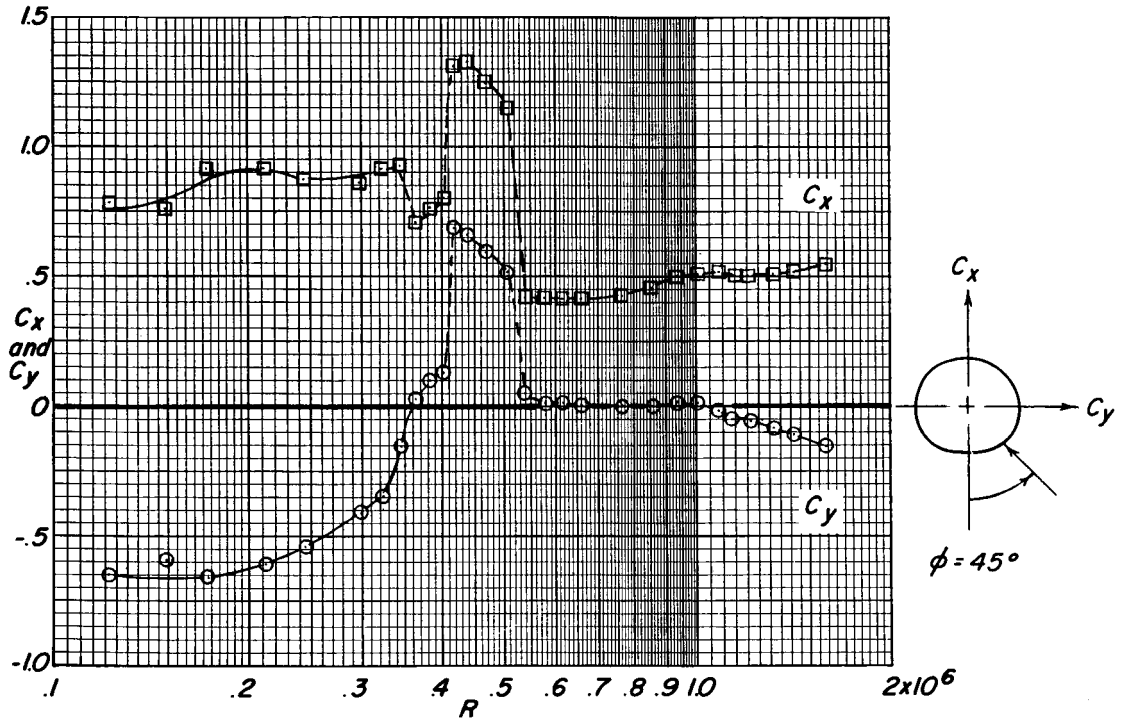

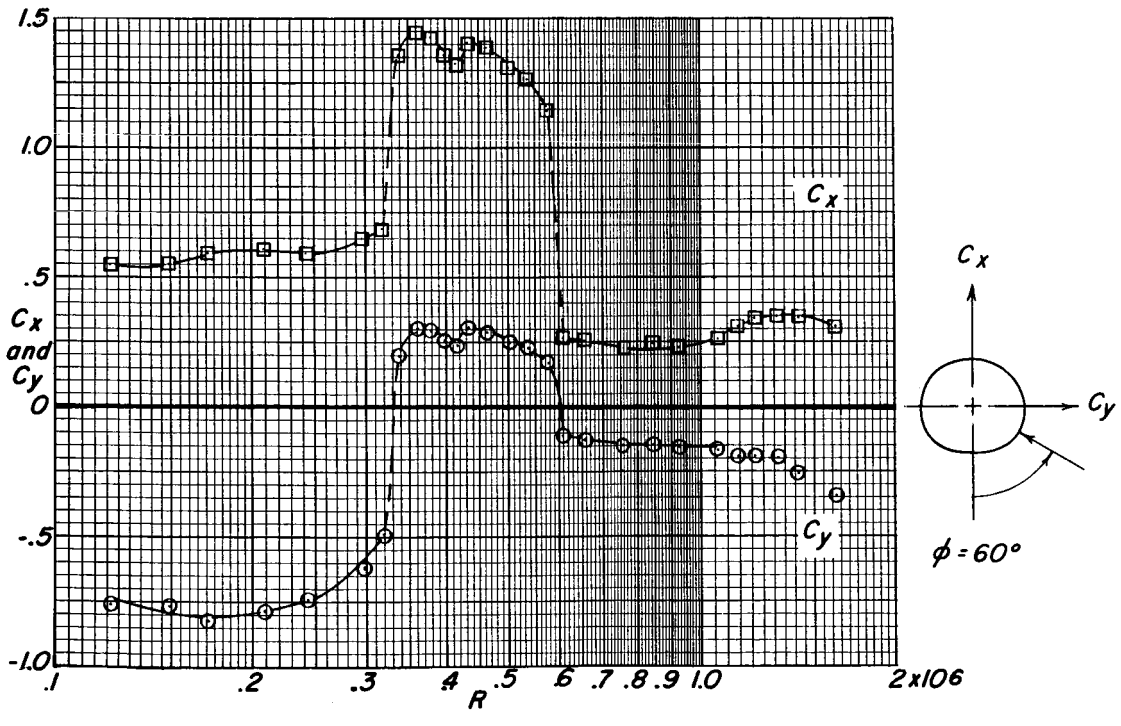

(d) $\Phi = 45^0$ and 60^0.

Figure 4.- Continued.

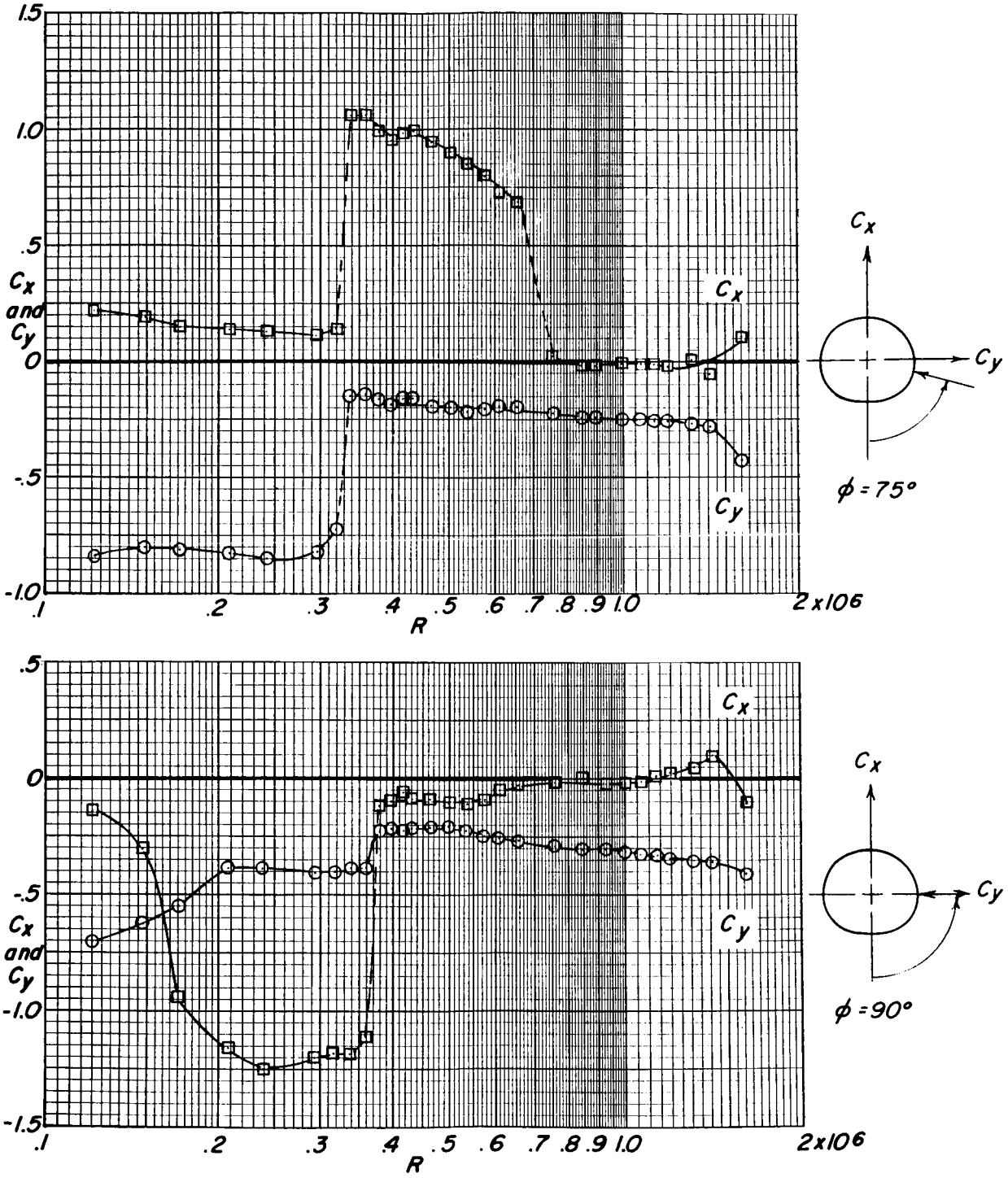

(e) $\Phi = 75^0$ and 90^0.

Figure 4.- Continued.

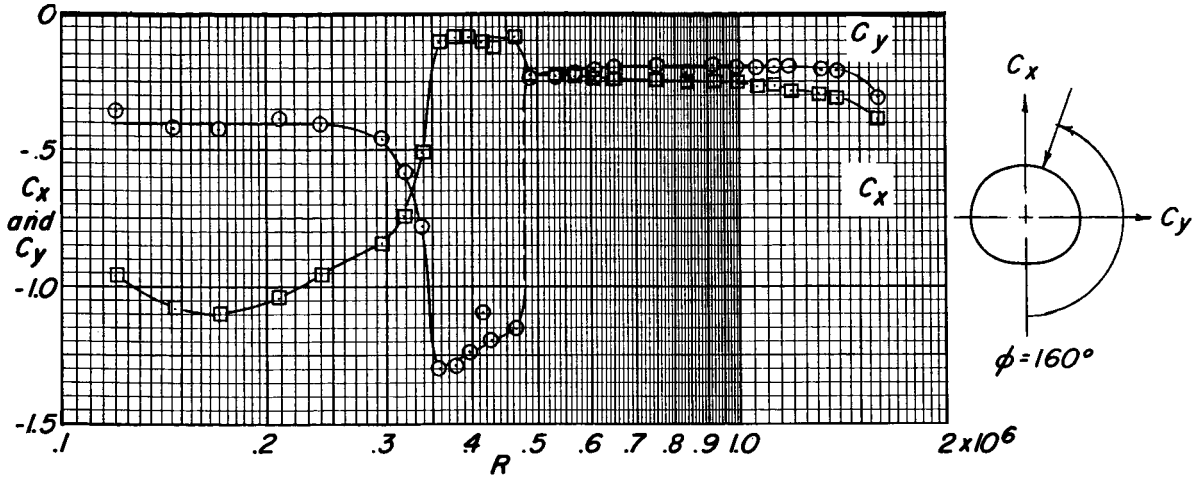

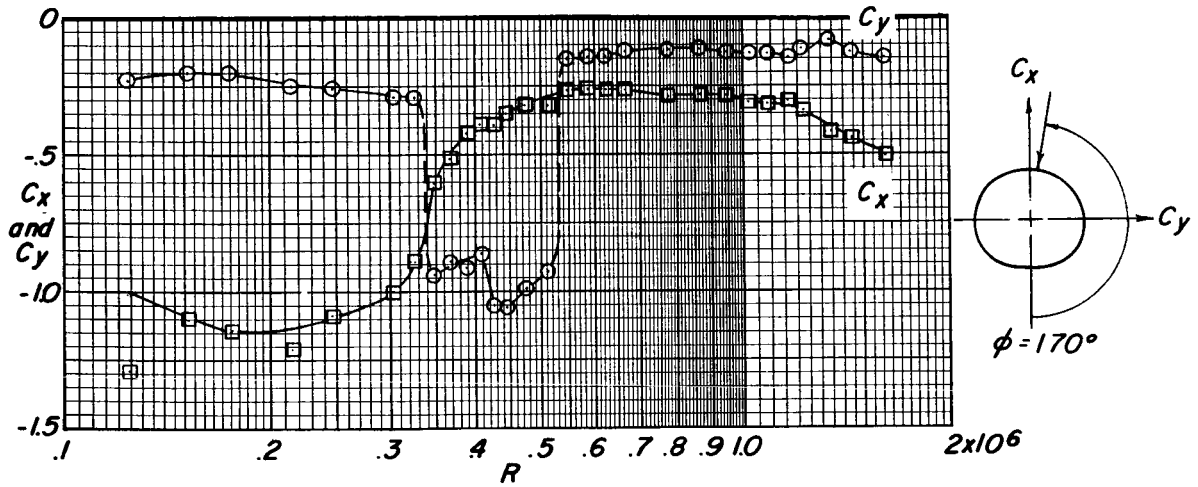

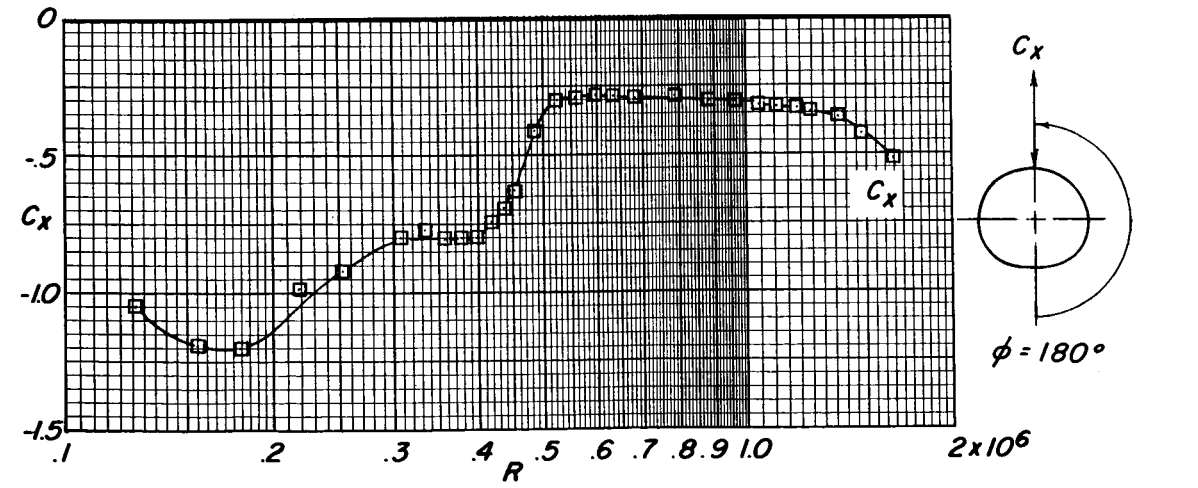

(f) $\Phi = 160^0$, 170^0, and 180^0.

Figure 4.- Concluded.

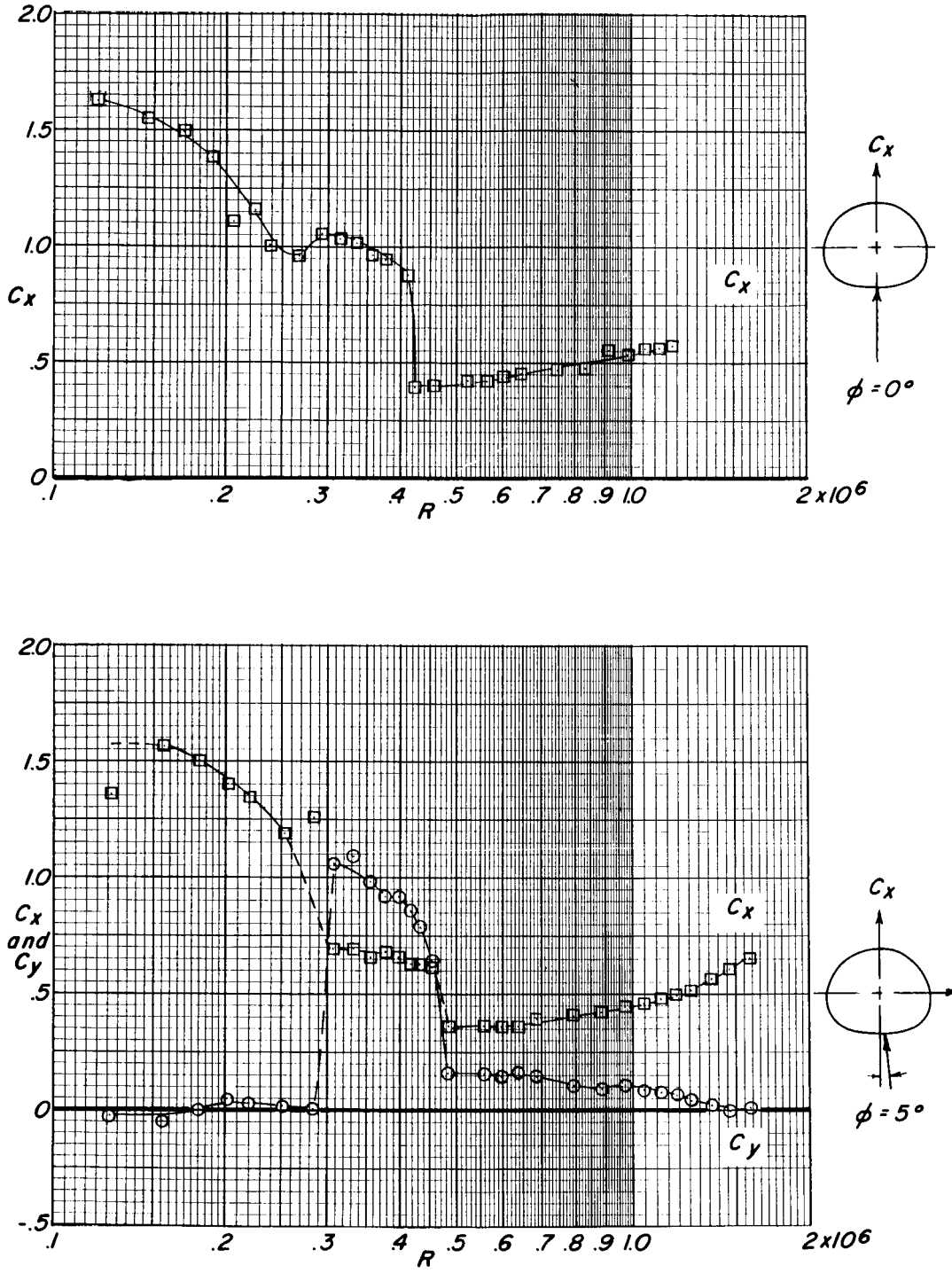

(a) $\Phi = 0^0$ and 5^0.

Figure 5.- Effect of Reynolds number at constant flow incidence on the force characteristics of cylinder B.

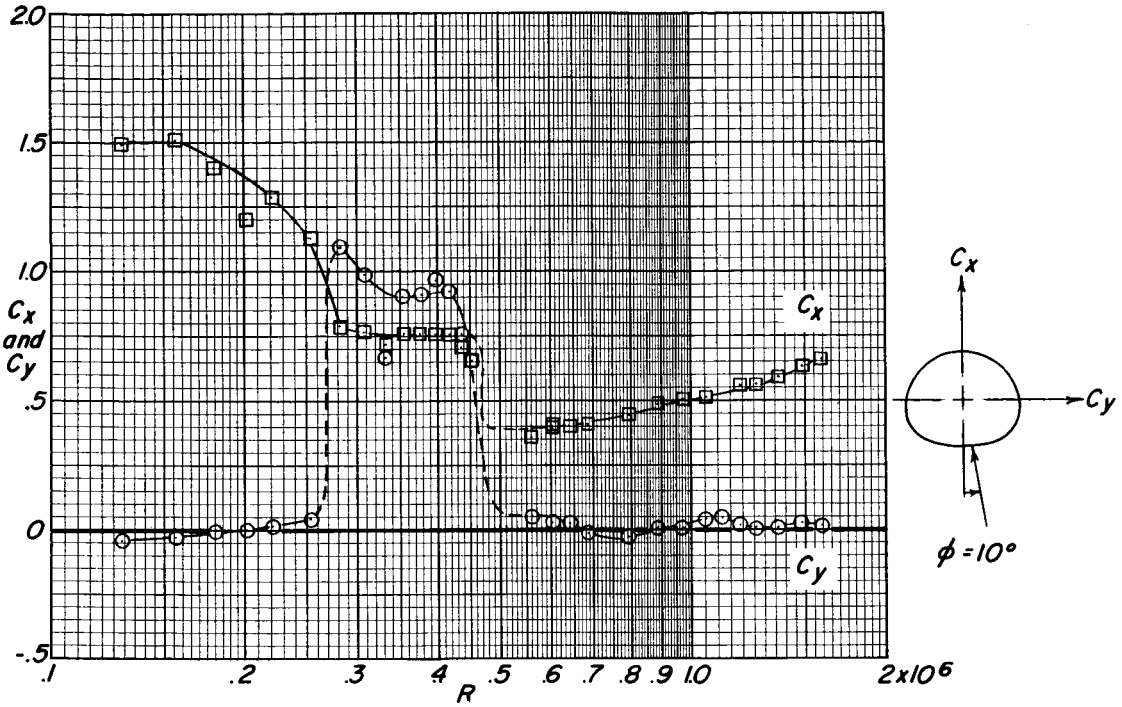

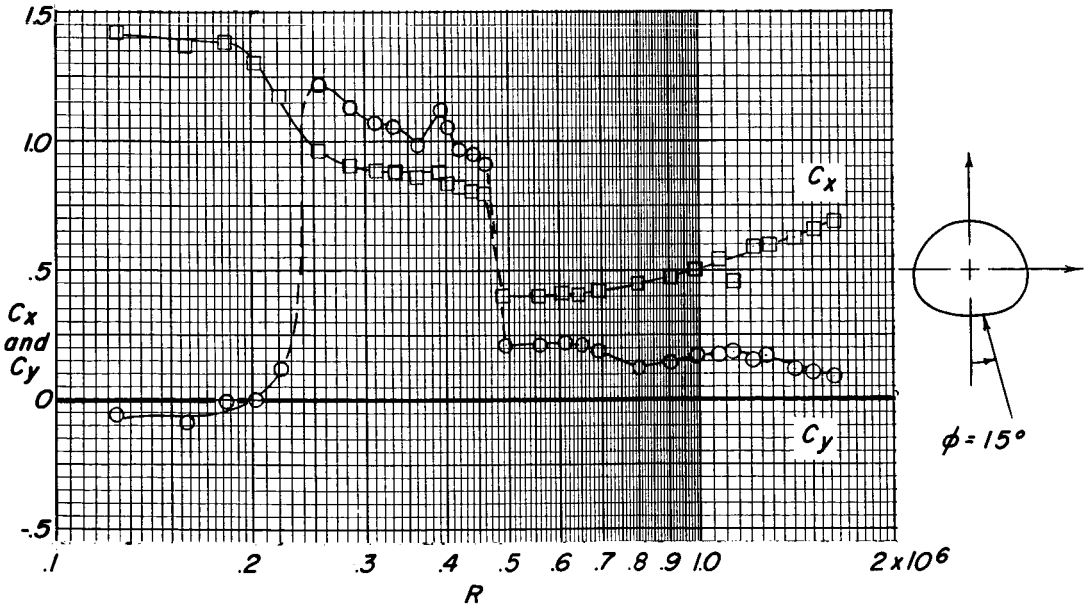

(b) $\Phi = 10^0$ and 15^0.

Figure 5.- Continued.

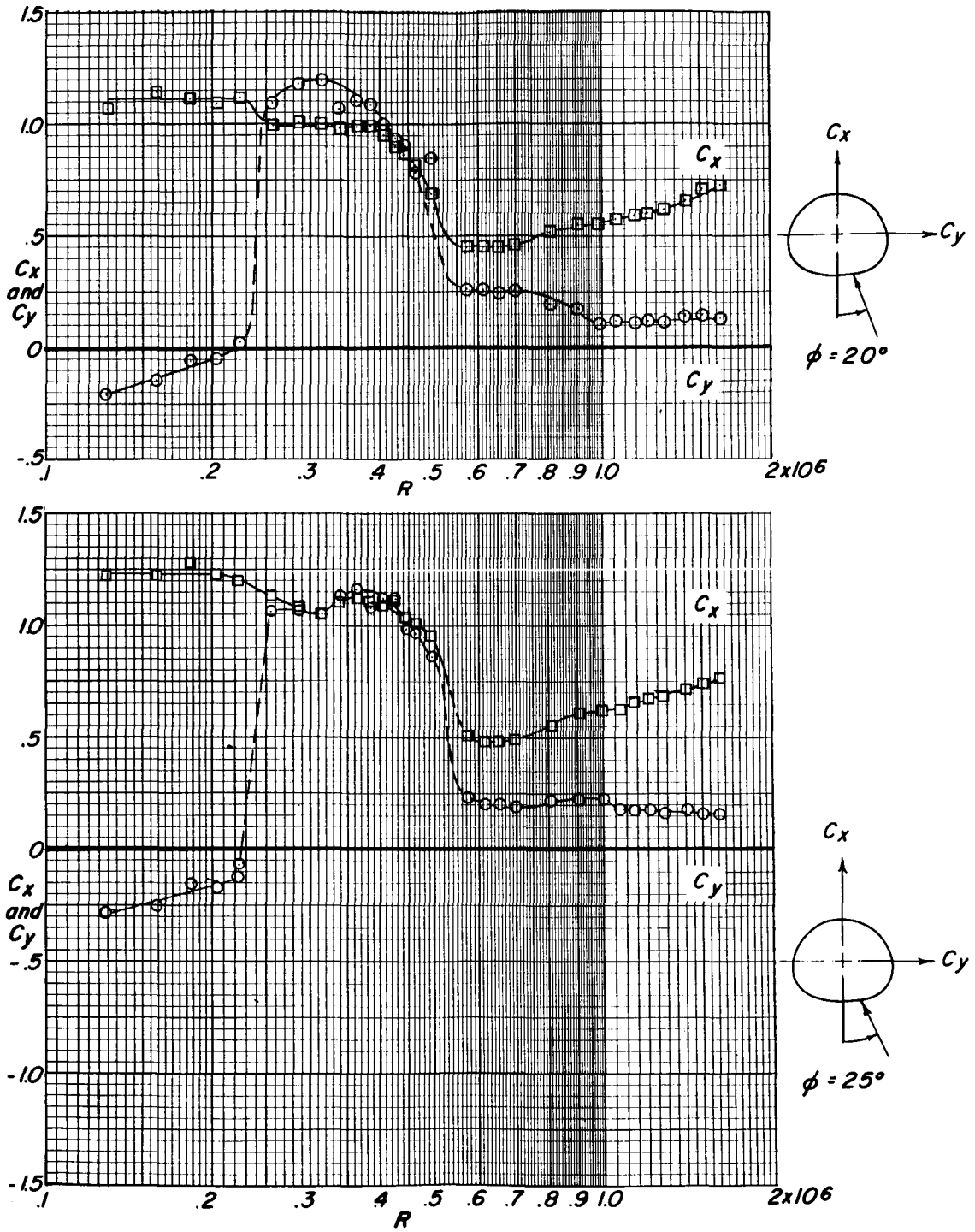

(c) $\Phi = 20^0$ and 25^0.

Figure 5.- Continued.

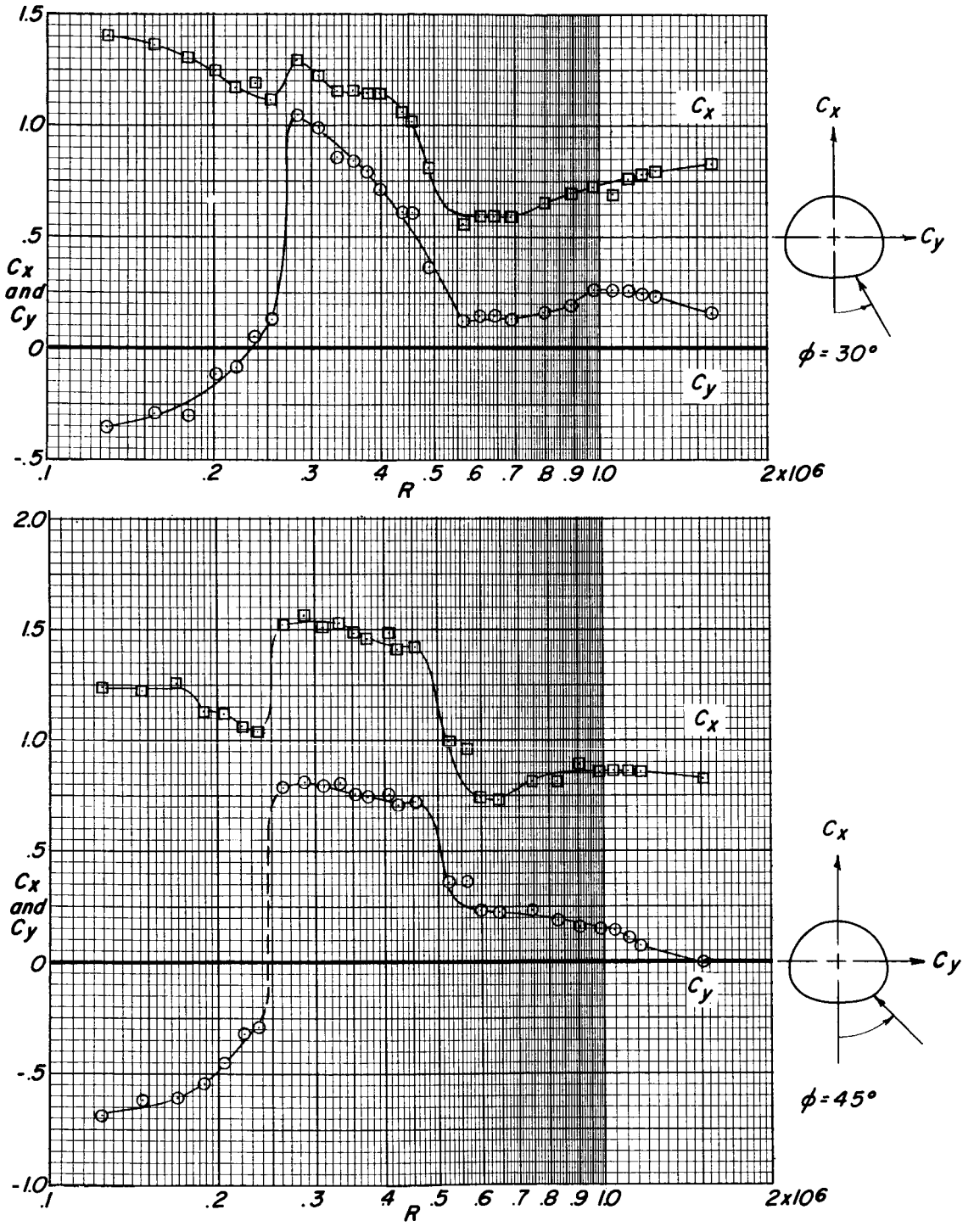

(d) $\Phi = 30^0$ and 45^0.

Figure 5.- Continued.

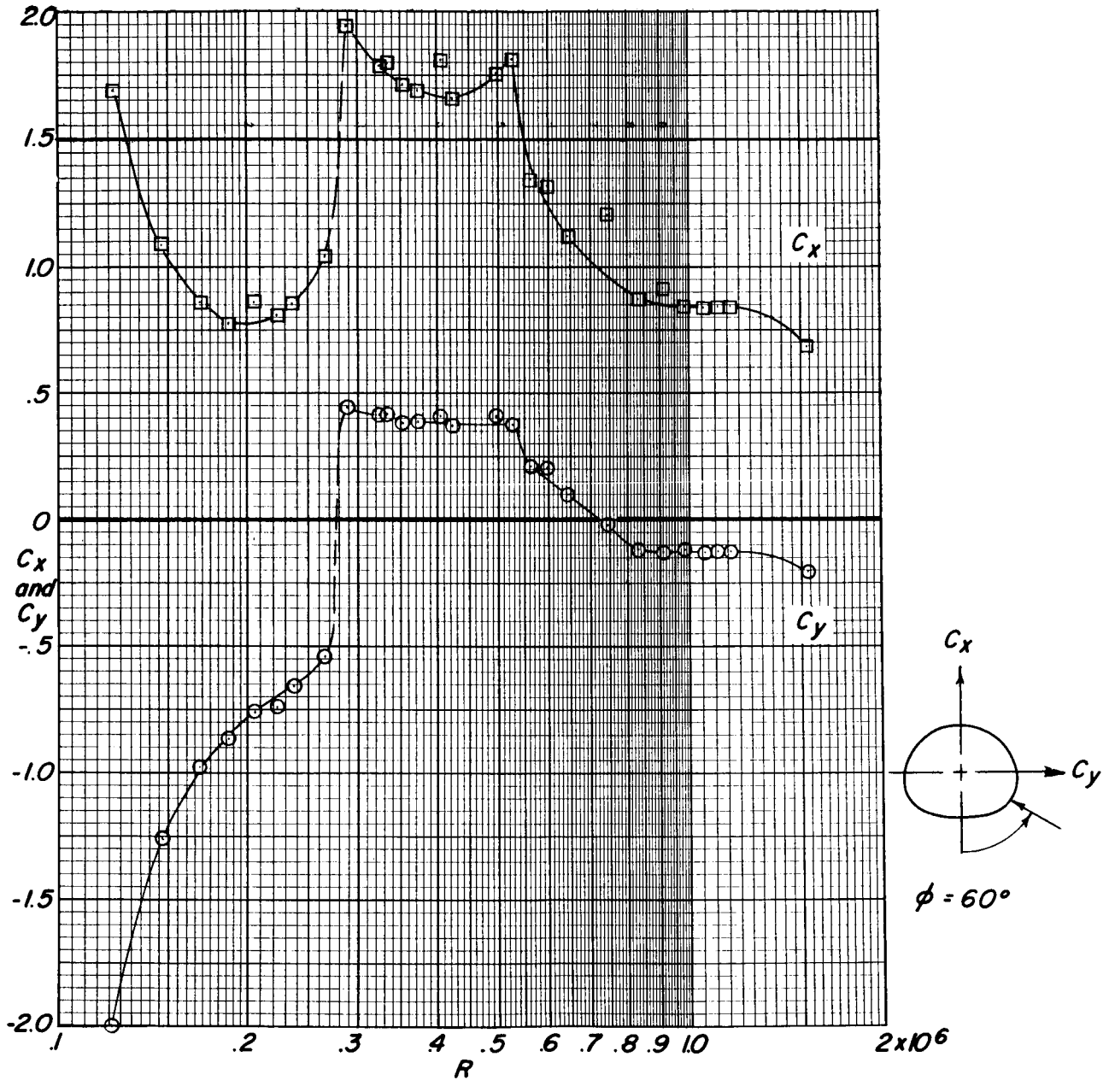

(e) $\Phi = 60^0$.

Figure 5.- Continued.

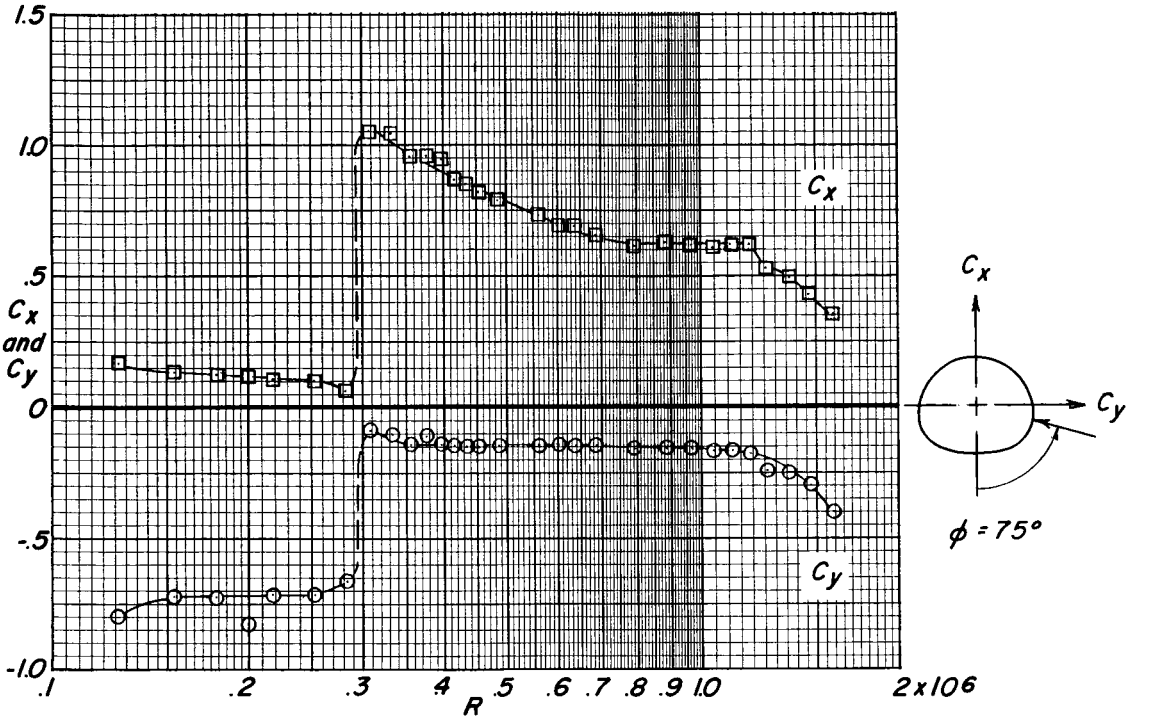

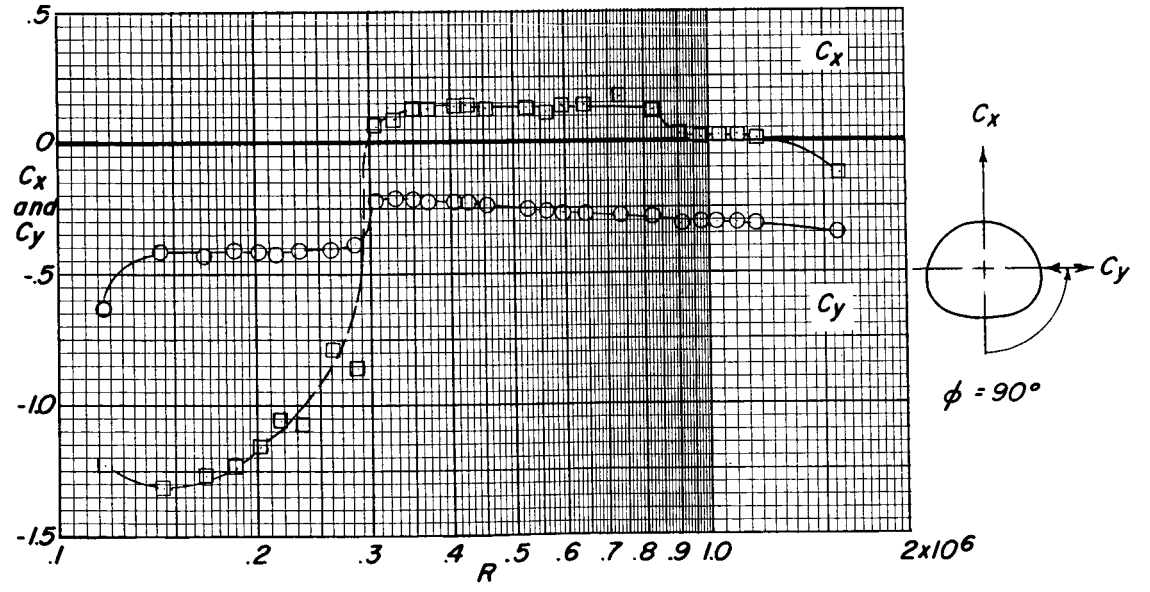

(f) $\Phi = 75^0$ and 90^0.

Figure 5.- Continued.

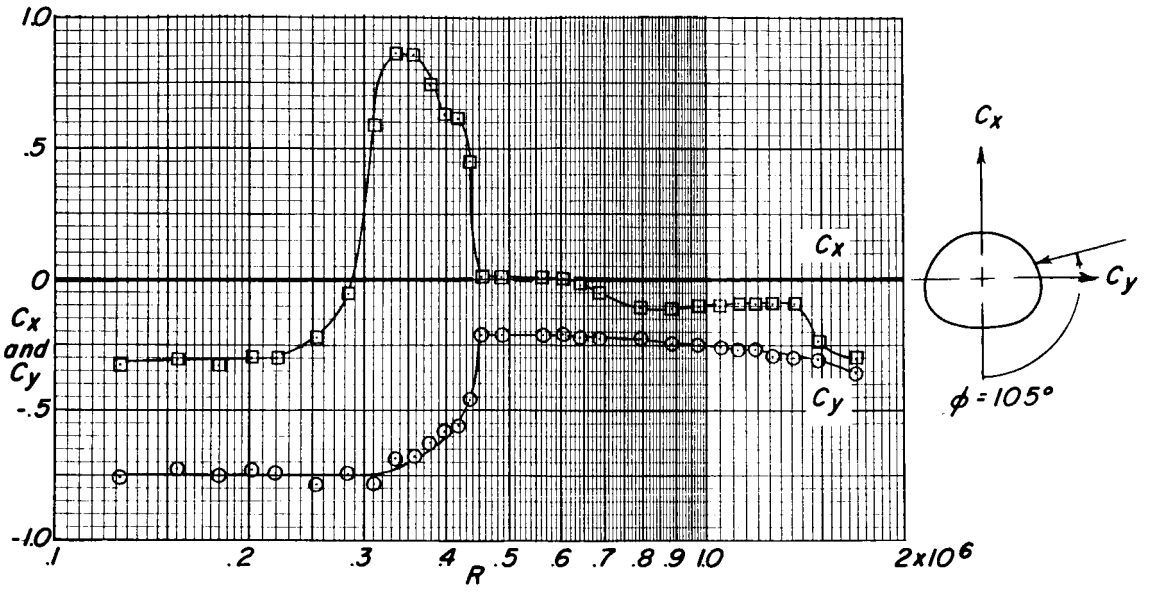

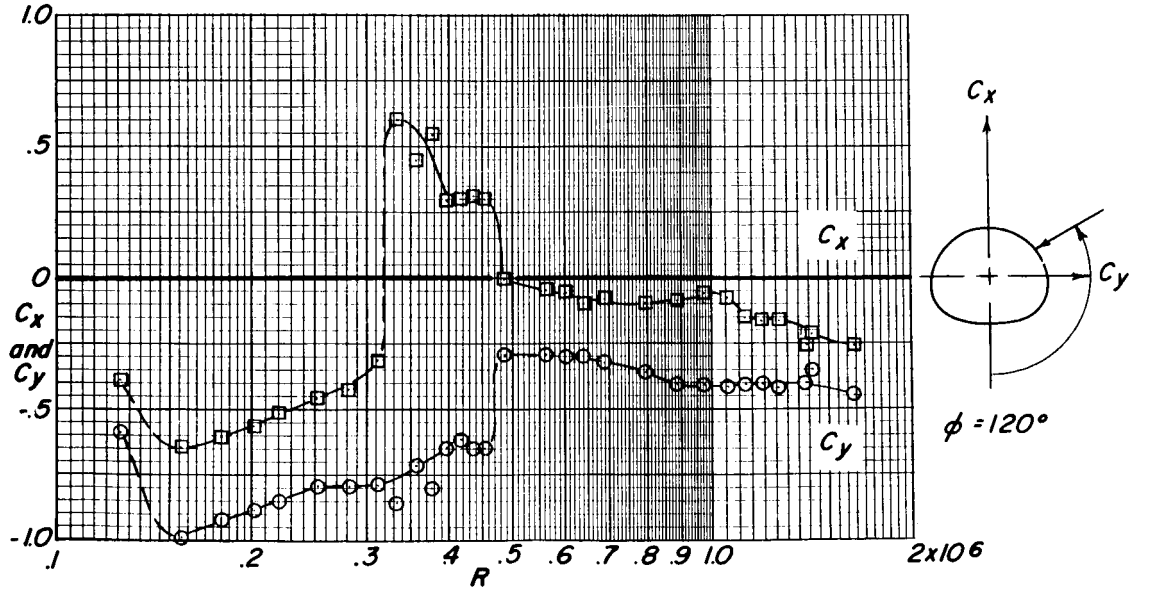

(g) $\Phi = 105^0$ and 120^0.

Figure 5.- Continued.

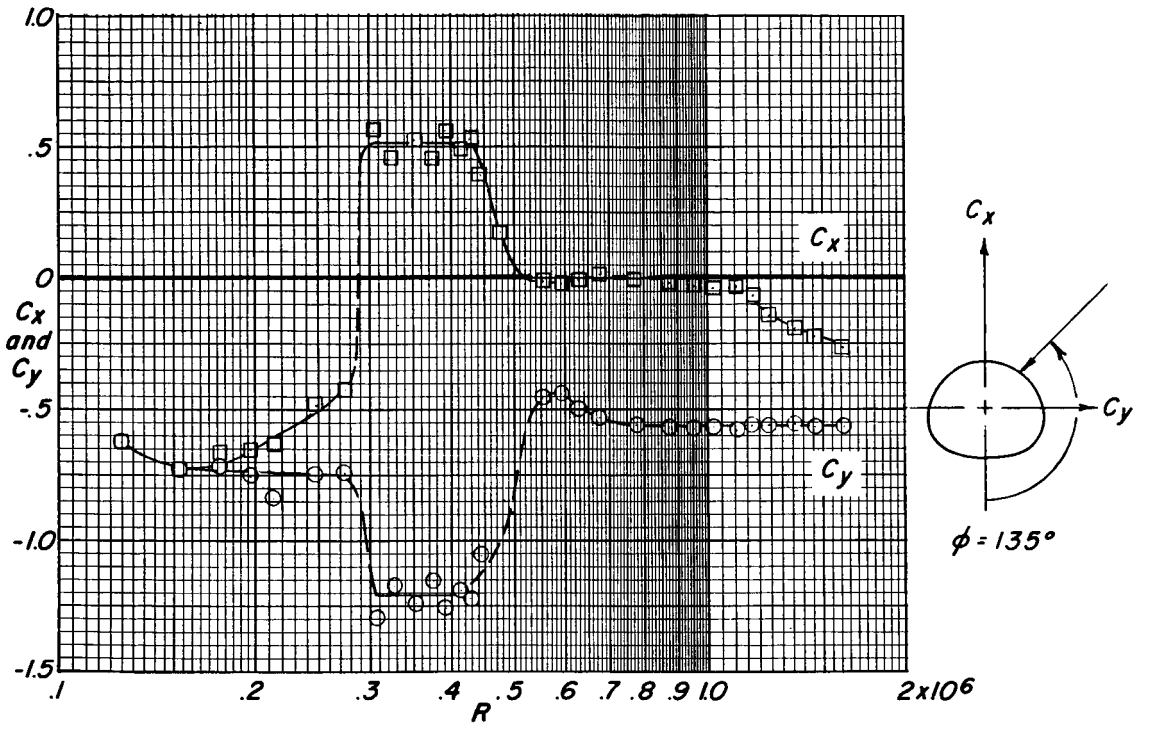

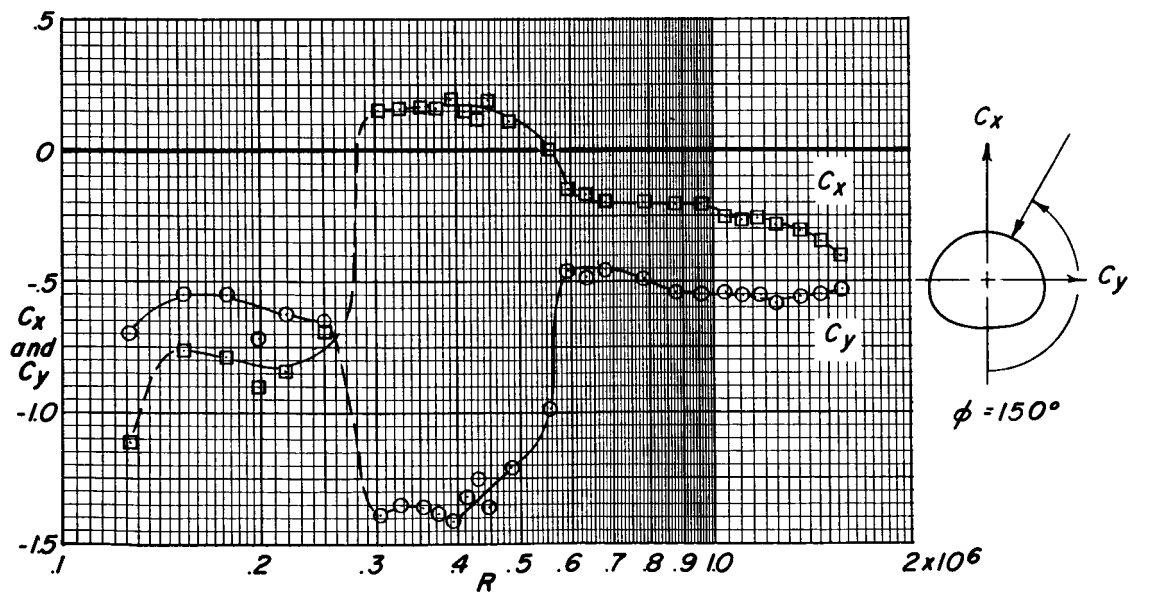

(h) $\Phi = 135^0$ and 150^0.

Figure 5.- Continued.

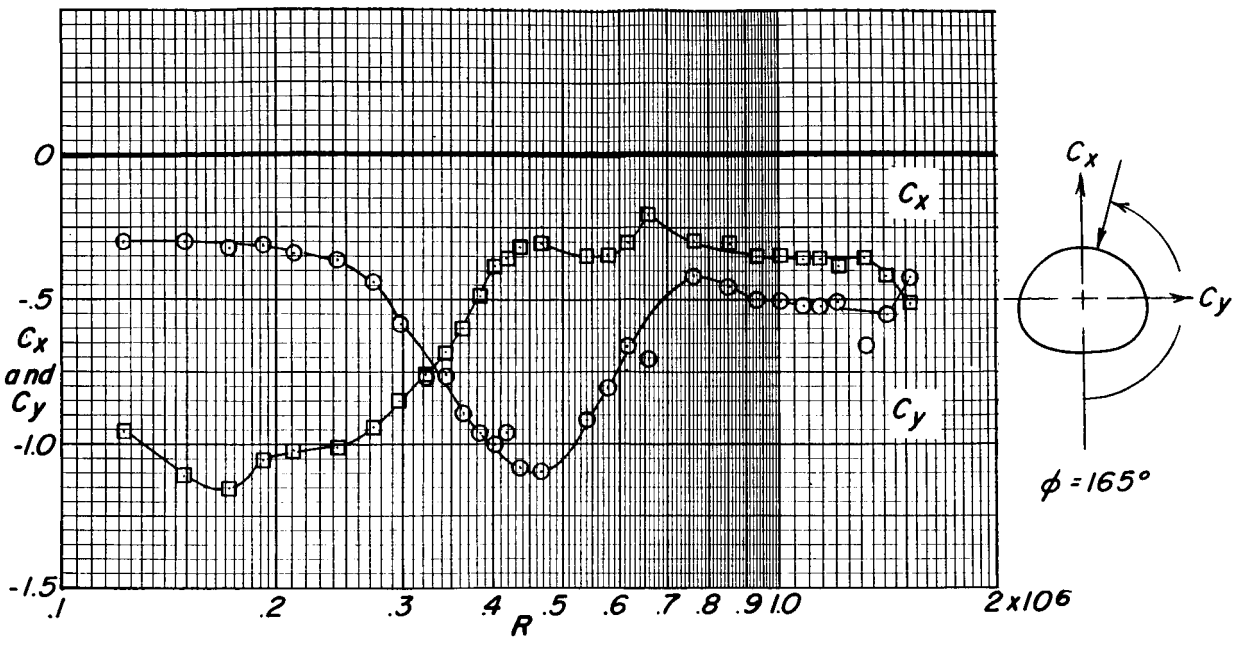

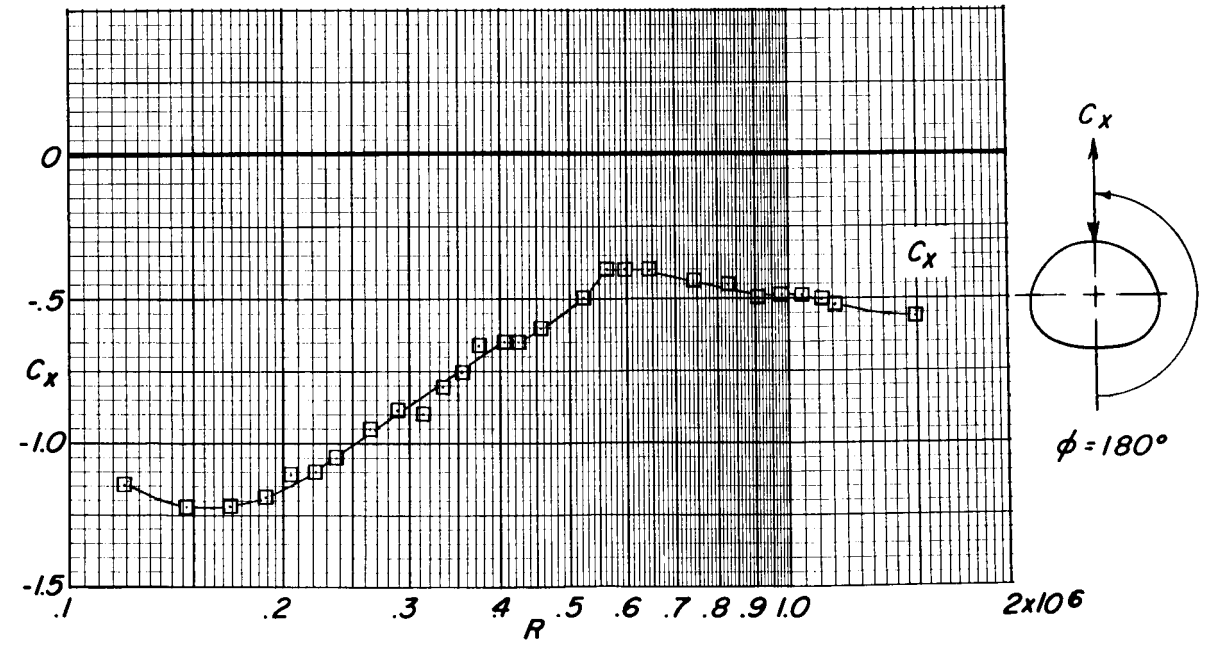

(i) $\Phi = 165^{0}$ and 180^{0}.

Figure 5.- Continued.

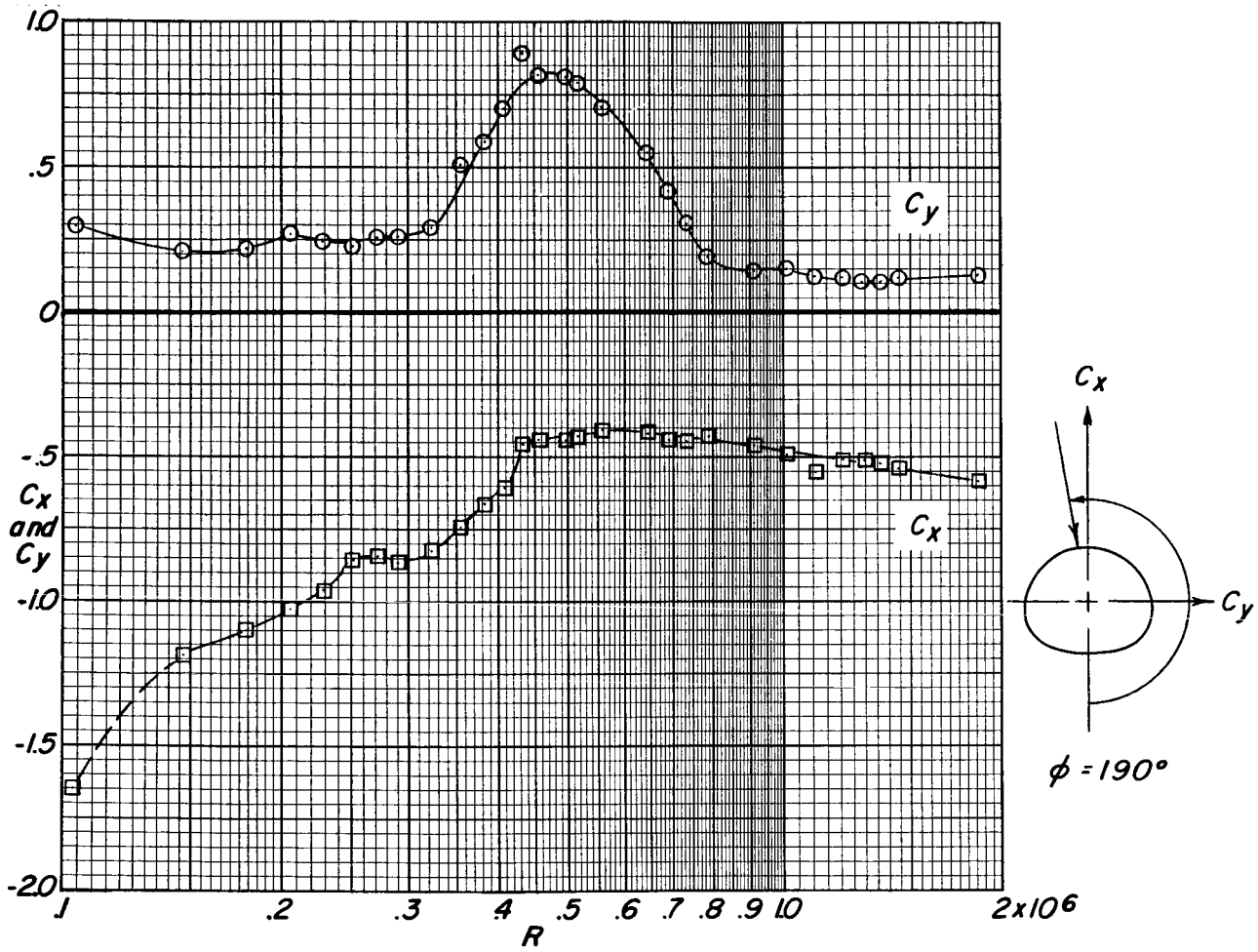

(j) $\Phi = 190^{0}$.

Figure 5.- Concluded.

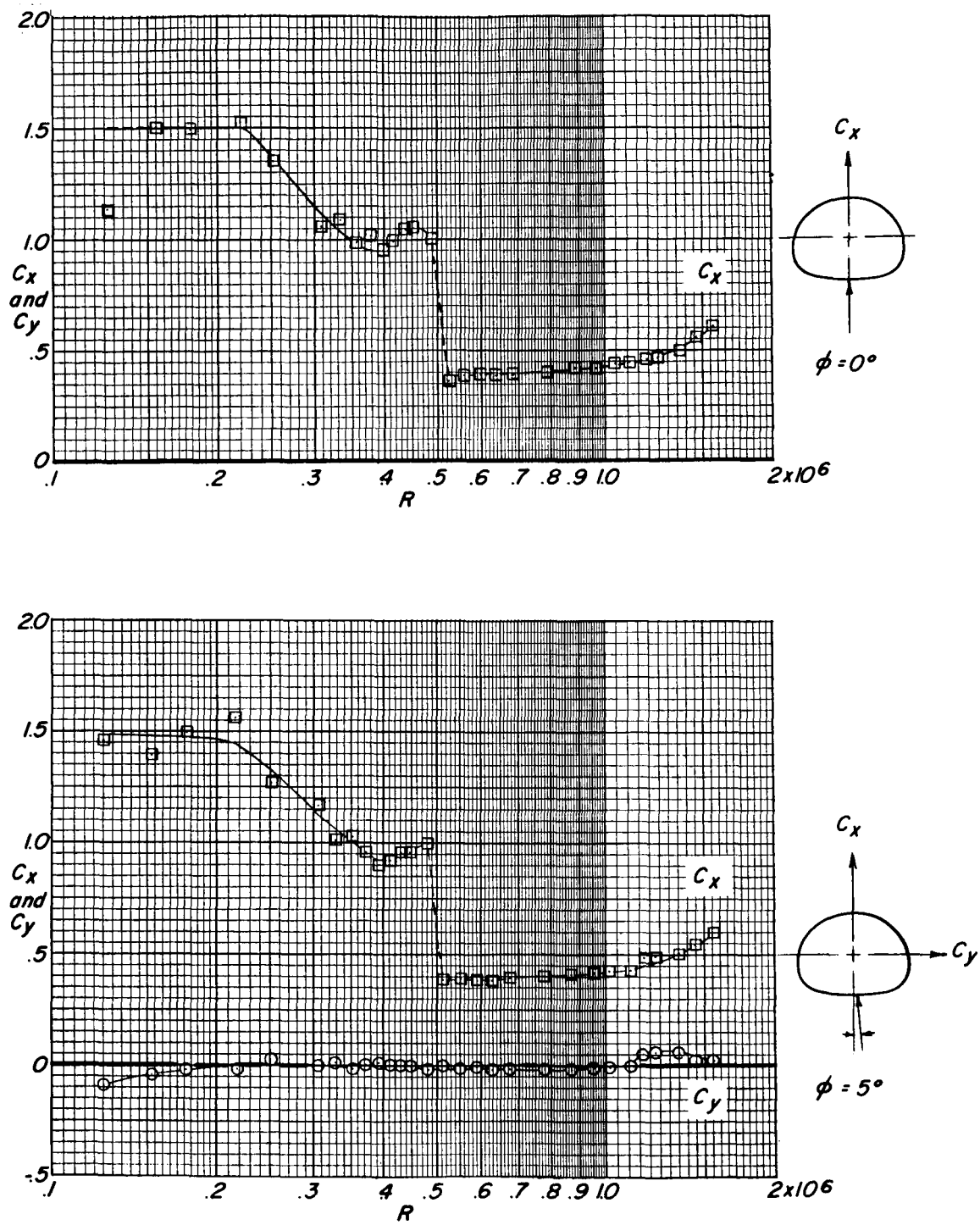

(a) $\Phi = 0^0$ and 5^0.

Figure 6.- Effect of Reynolds number at constant flow incidence on the force characteristics of cylinder C.

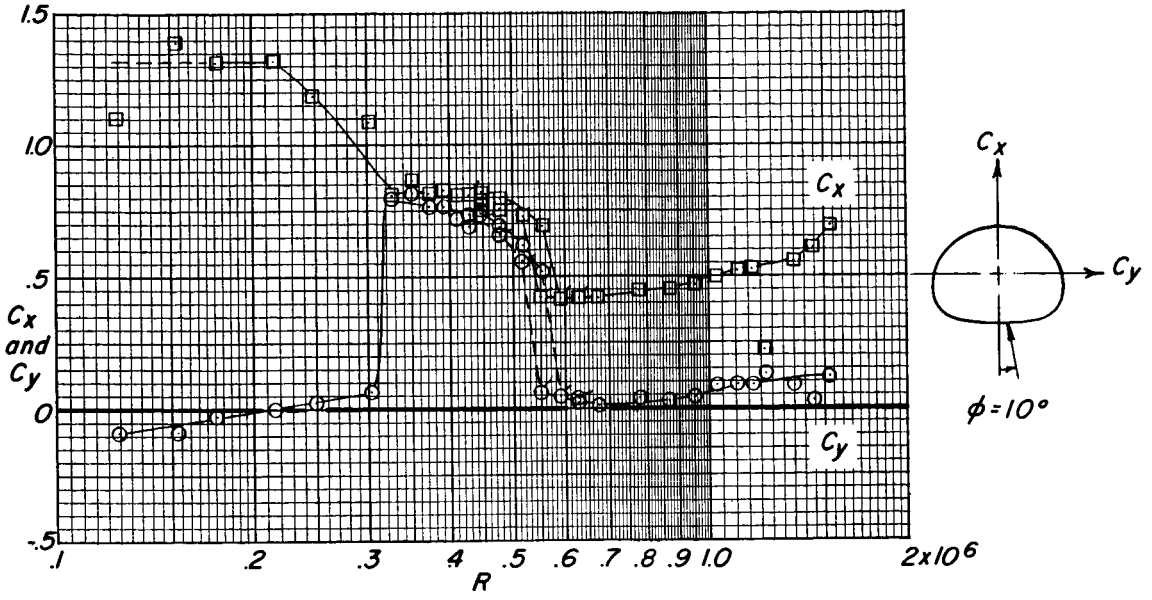

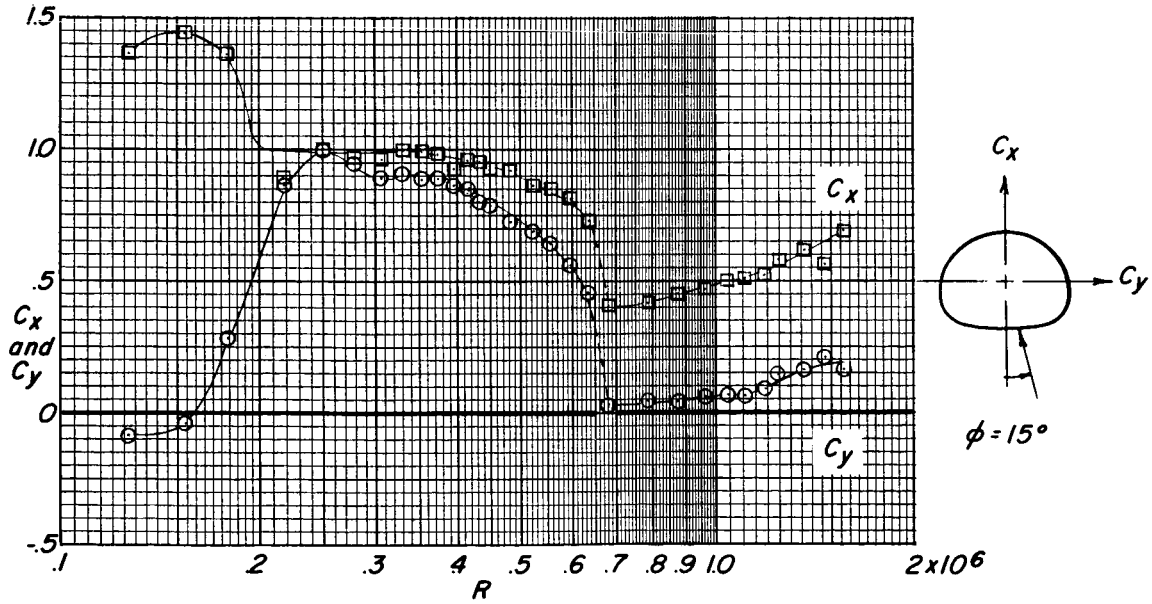

(b) $\Phi = 10^0$ and 15^0. (Flagged symbols indicate decreasing Reynolds numbers.)

Figure 6.- Continued.

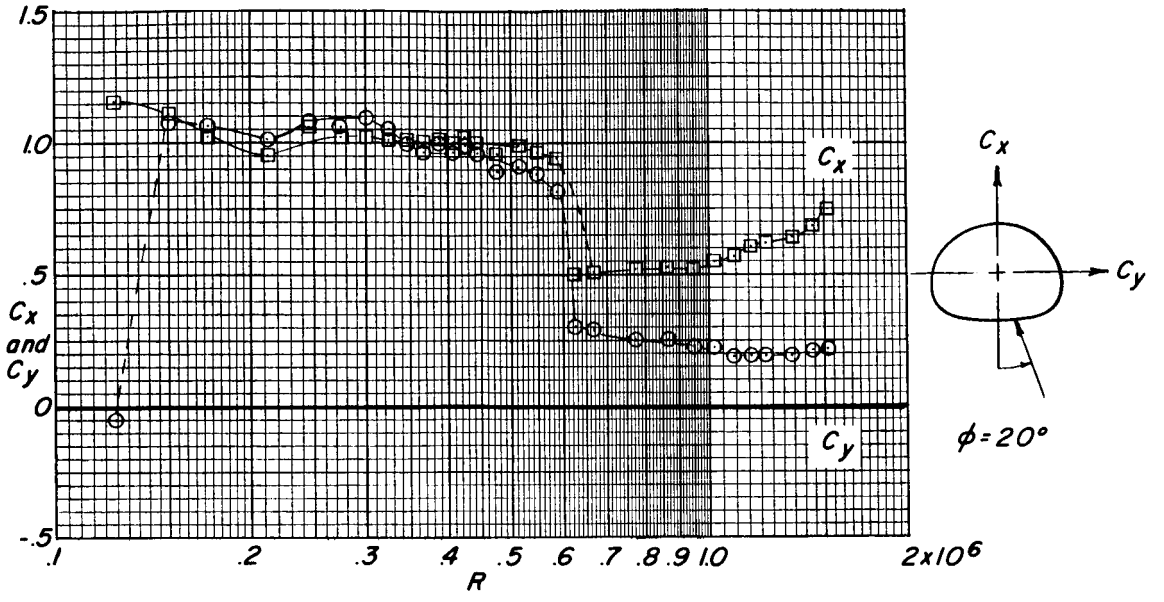

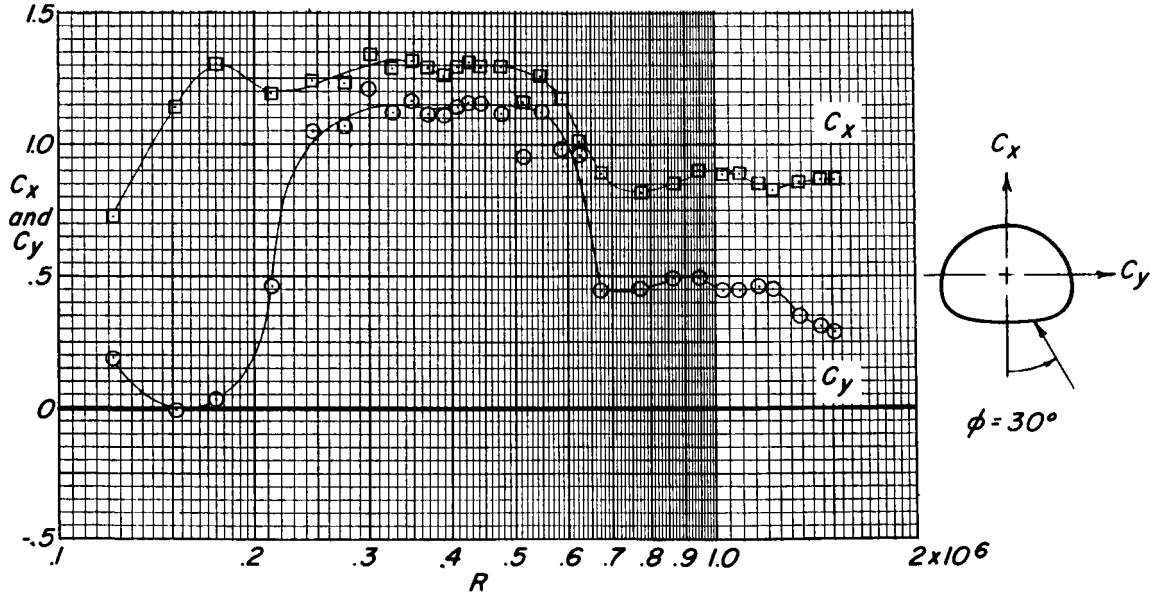

(c) $\Phi = 20^0$ and 30^0.

Figure 6.- Continued.

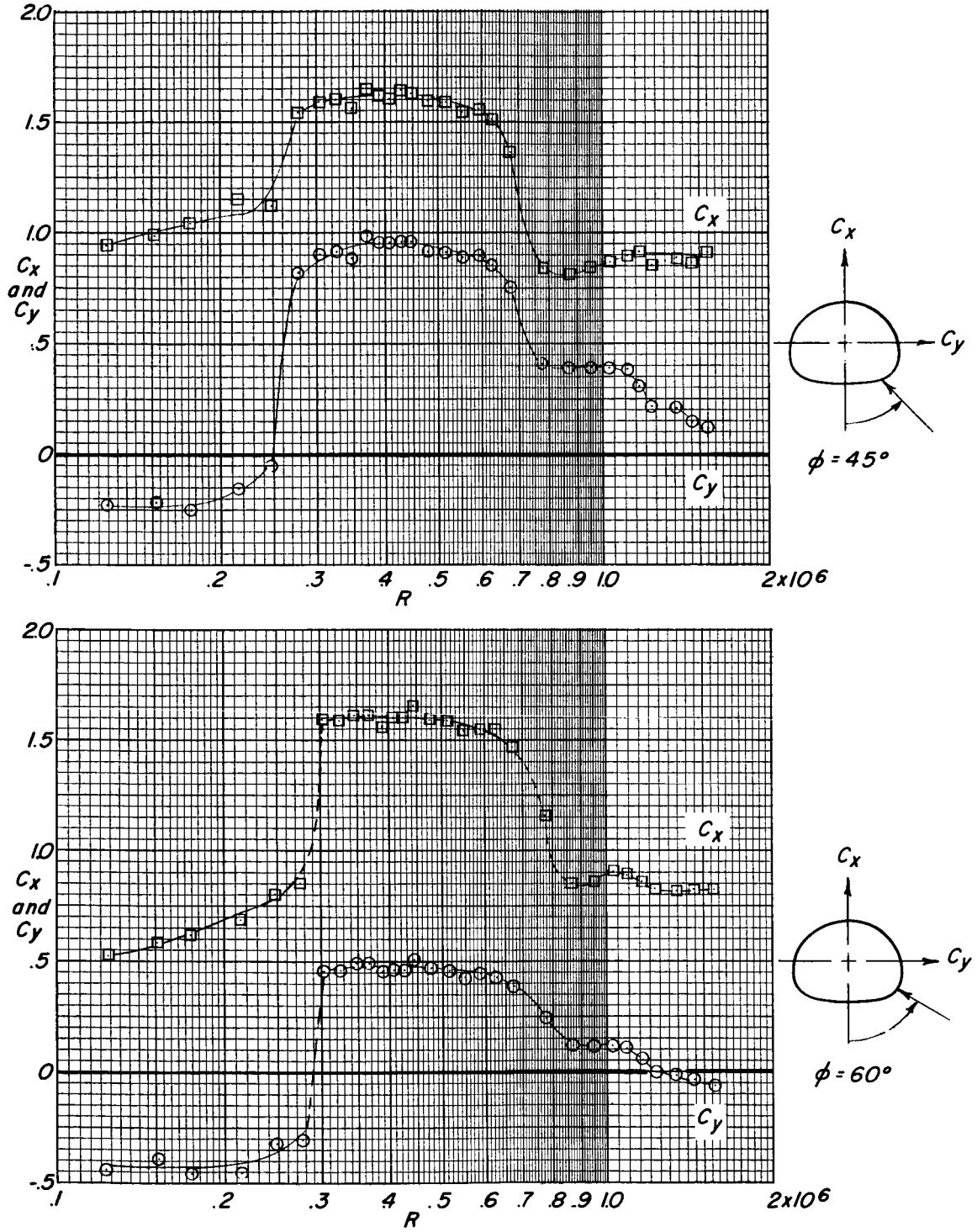

(d) $\Phi = 45^0$ and 60^0.

Figure 6.- Continued.

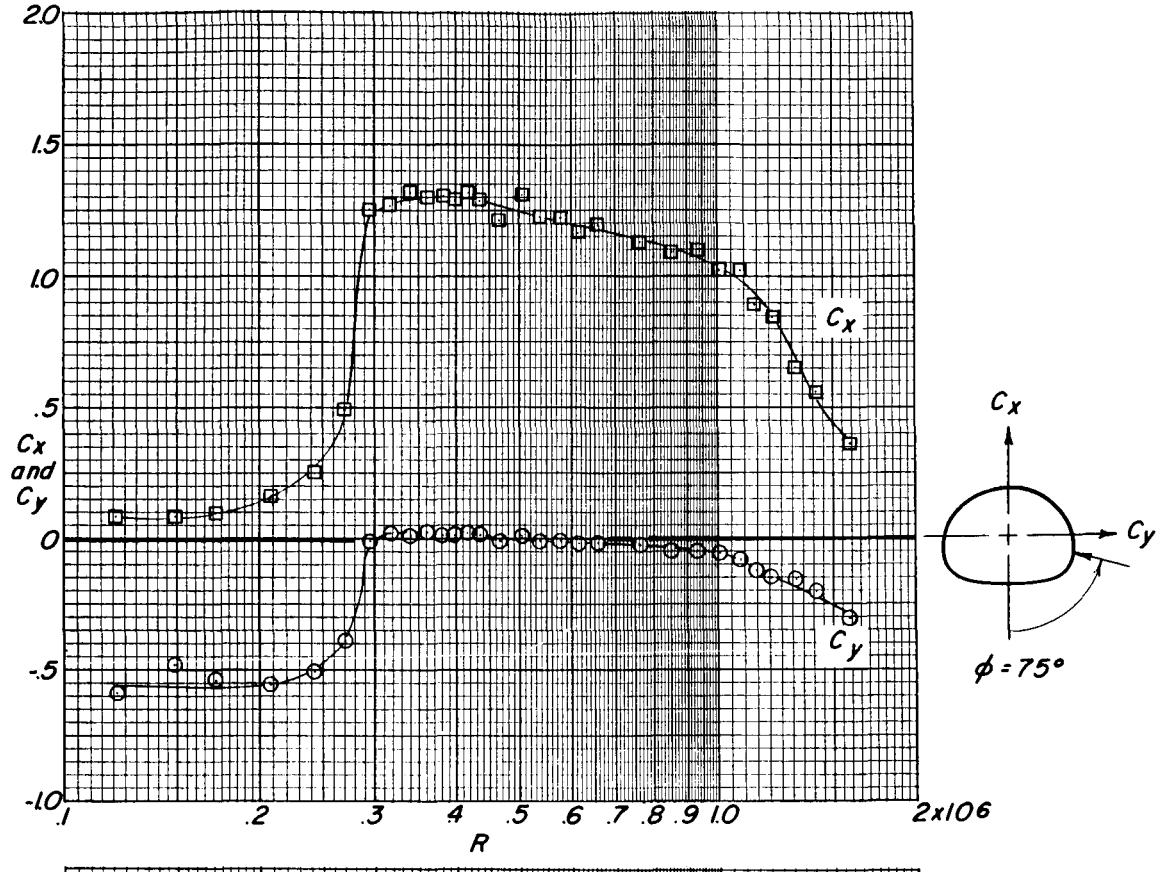

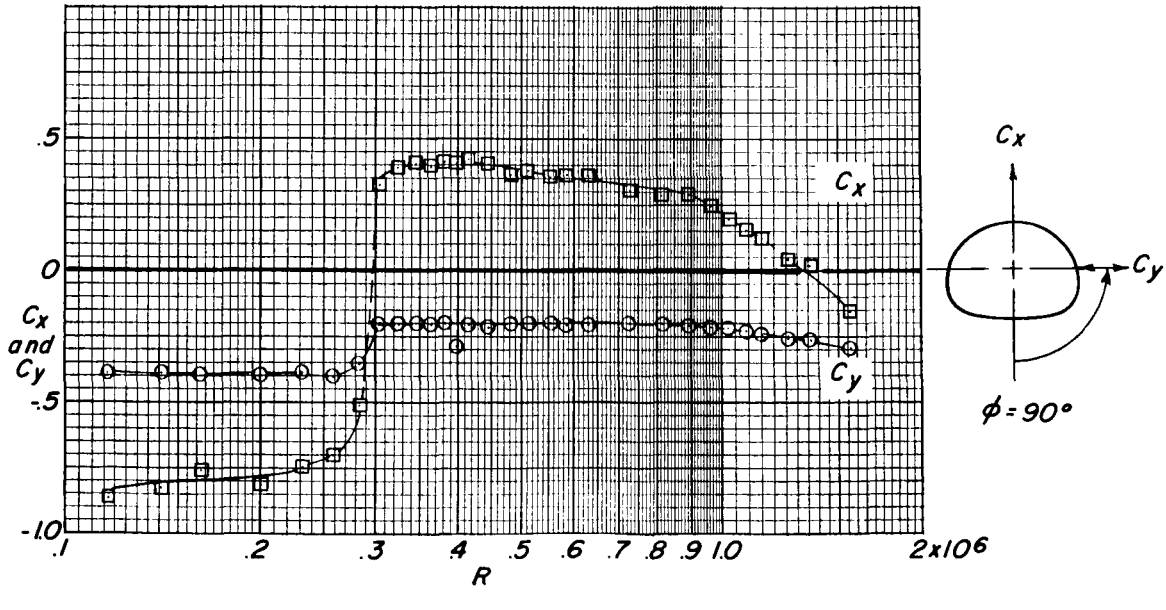

(e) $\Phi = 75^0$ and 90^0.

Figure 6.- Continued.

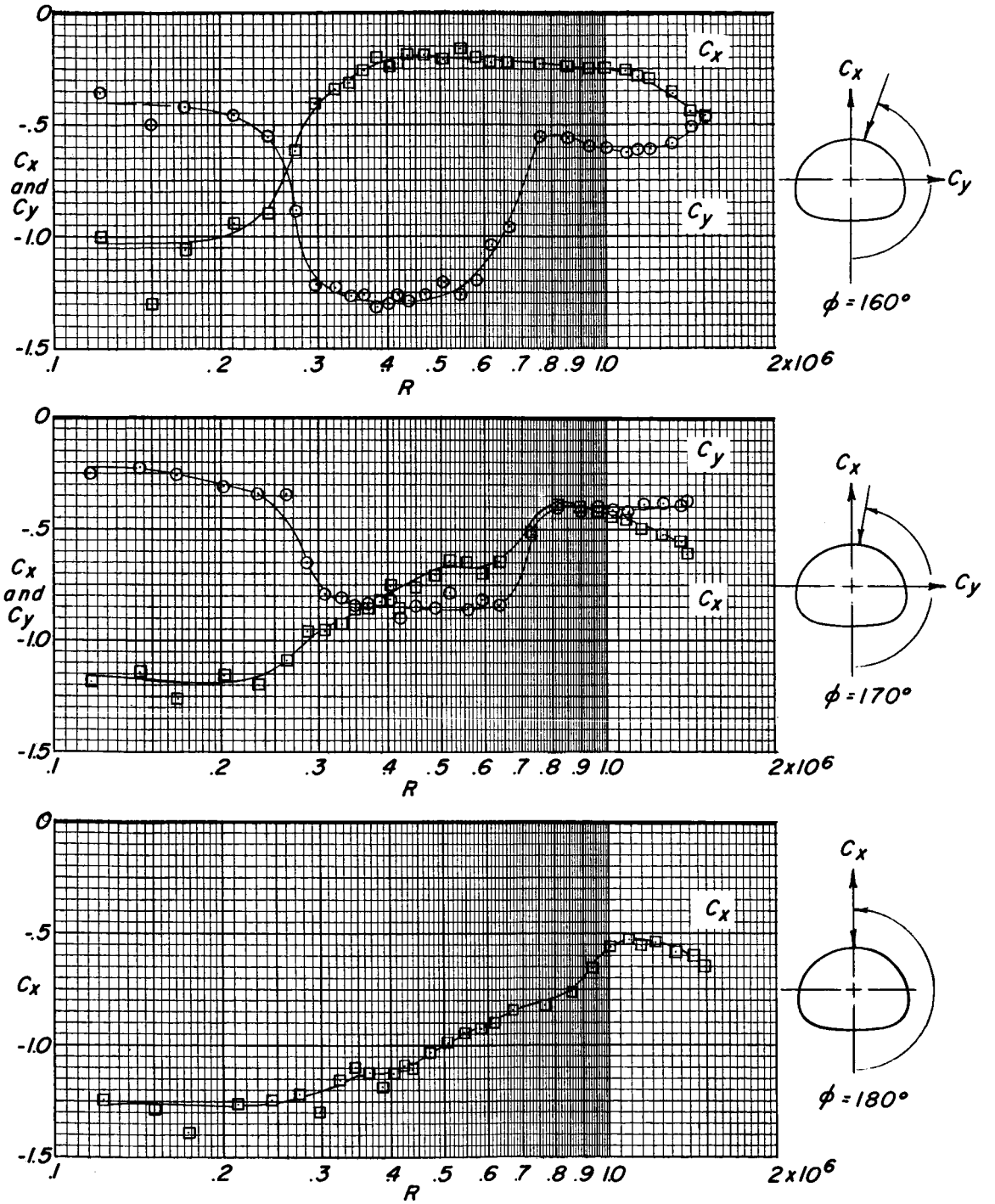

(f) $\Phi = 160^{0}$, 170^{0}, and 180^{0}.

Figure 6.- Concluded.

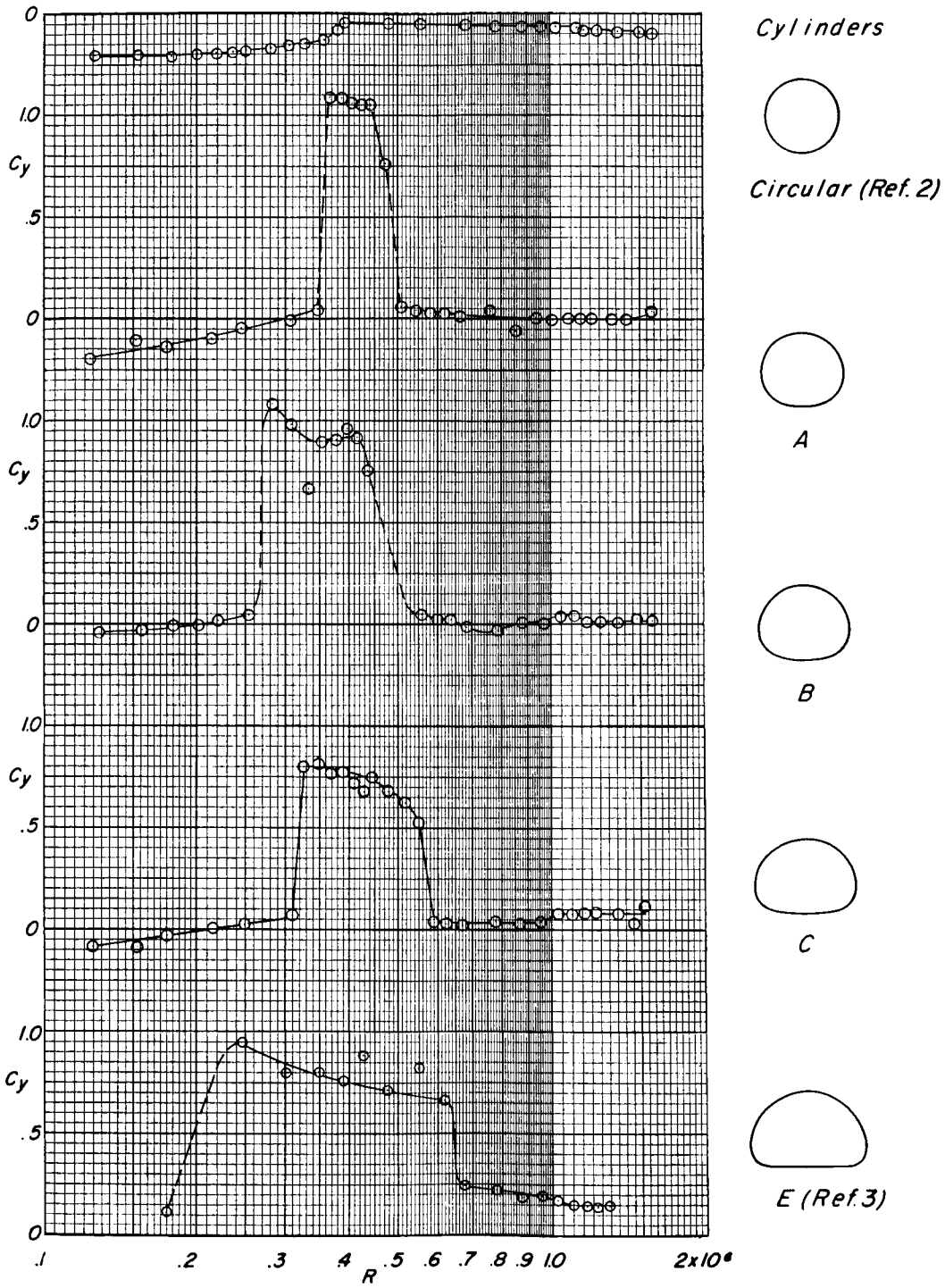

(a) c_y; $\Phi = 10^0$.

Figure 7.- Comparison of the force characteristics of various cylinders at $\Phi = 10^0$ and $\Phi = 30^0$.

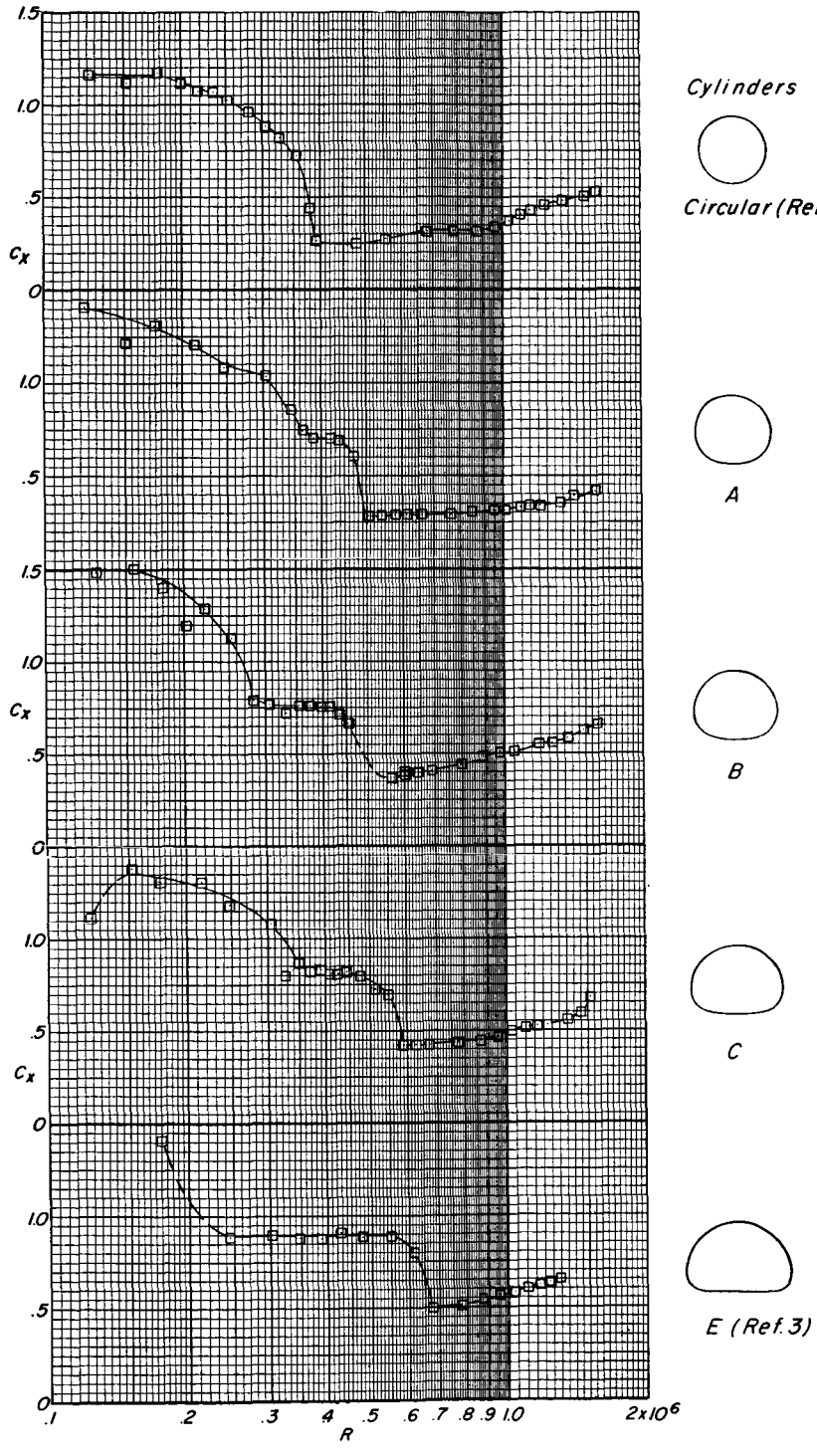

(b) c_X; $\Phi = 10^0$.

Figure 7.- Continued.

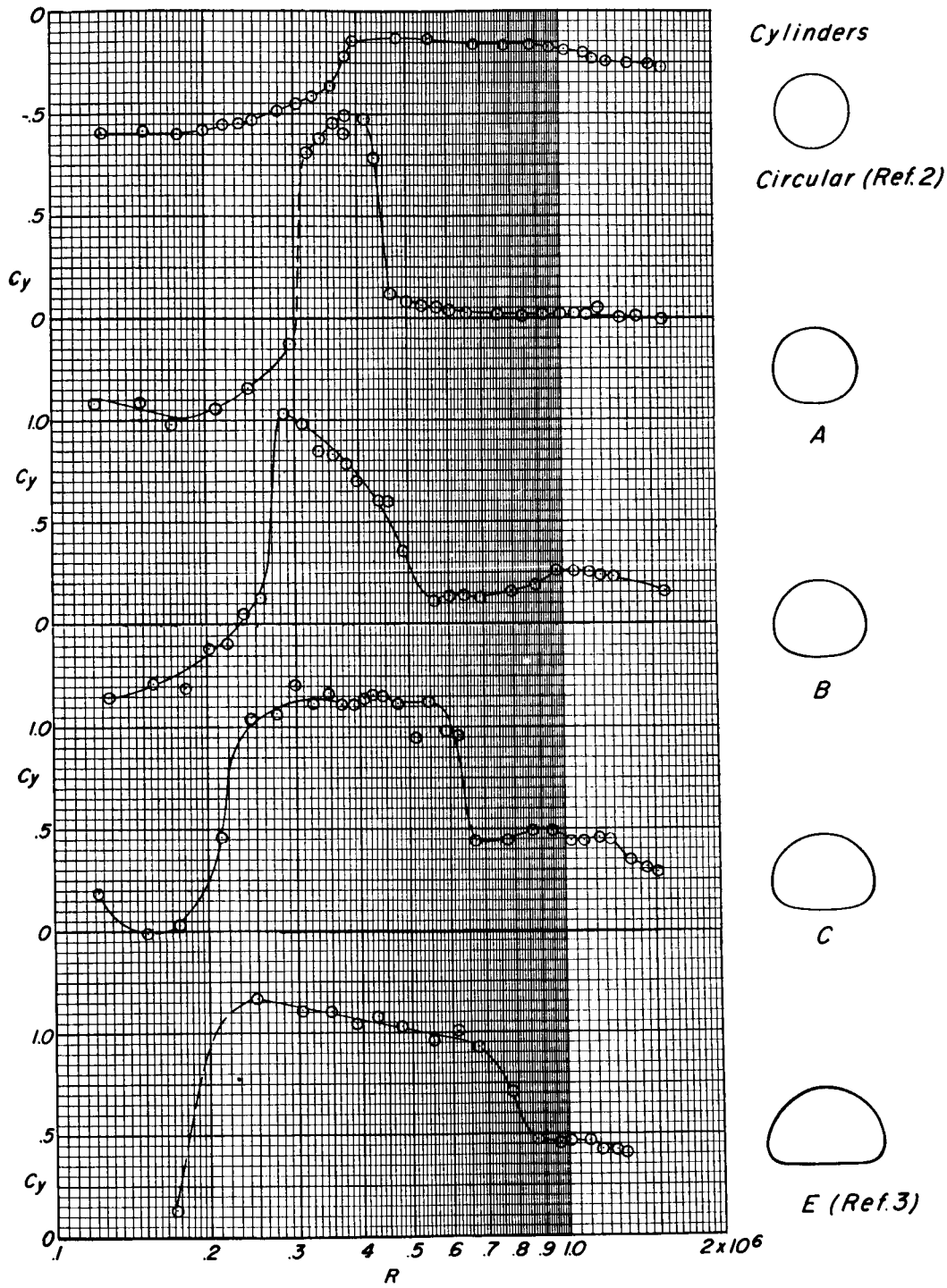

(c) c_y; $\Phi = 30^0$.

Figure 7.- Continued.

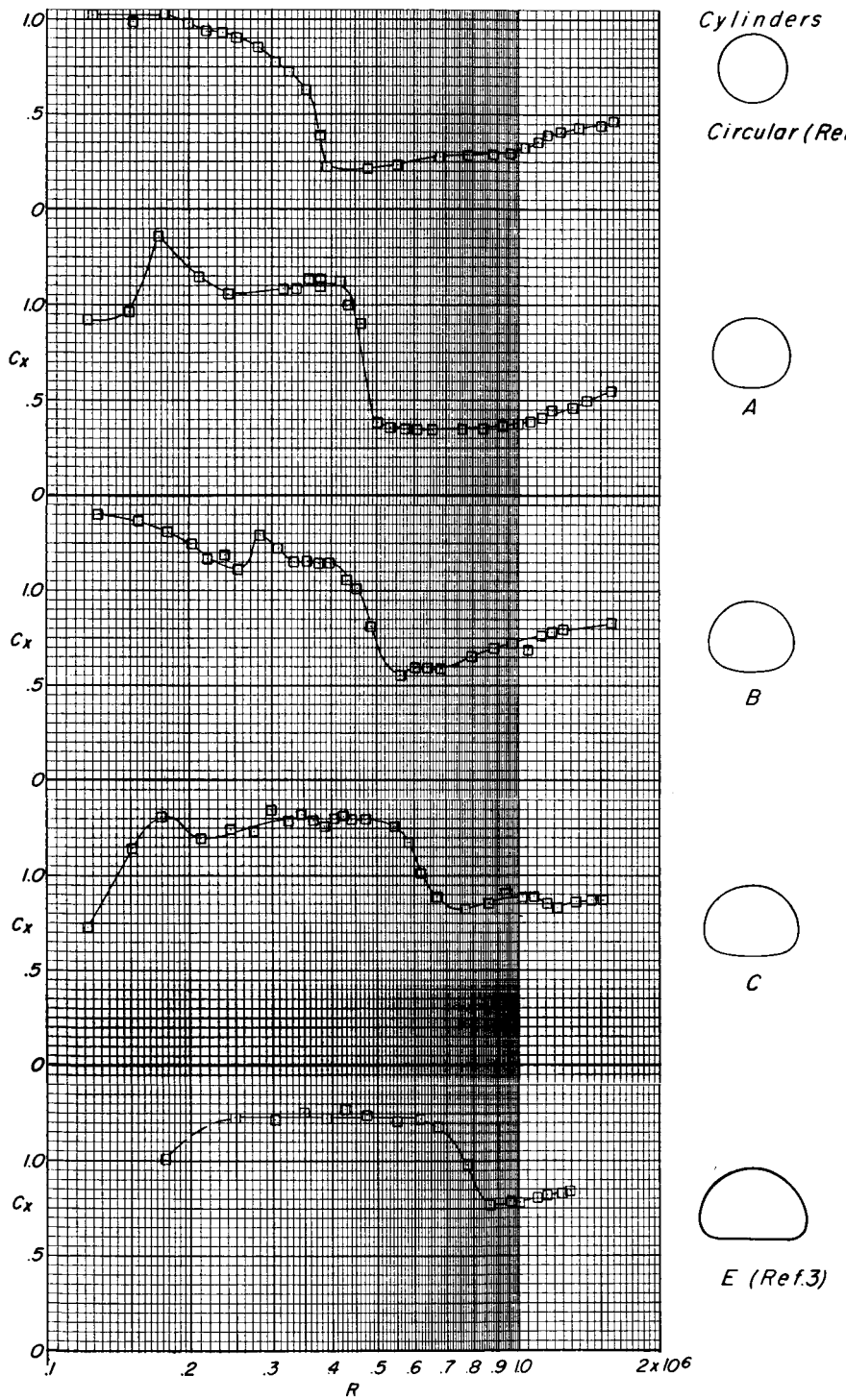

(d) c_x; $\Phi = 30^0$.

Figure 7.- Concluded.

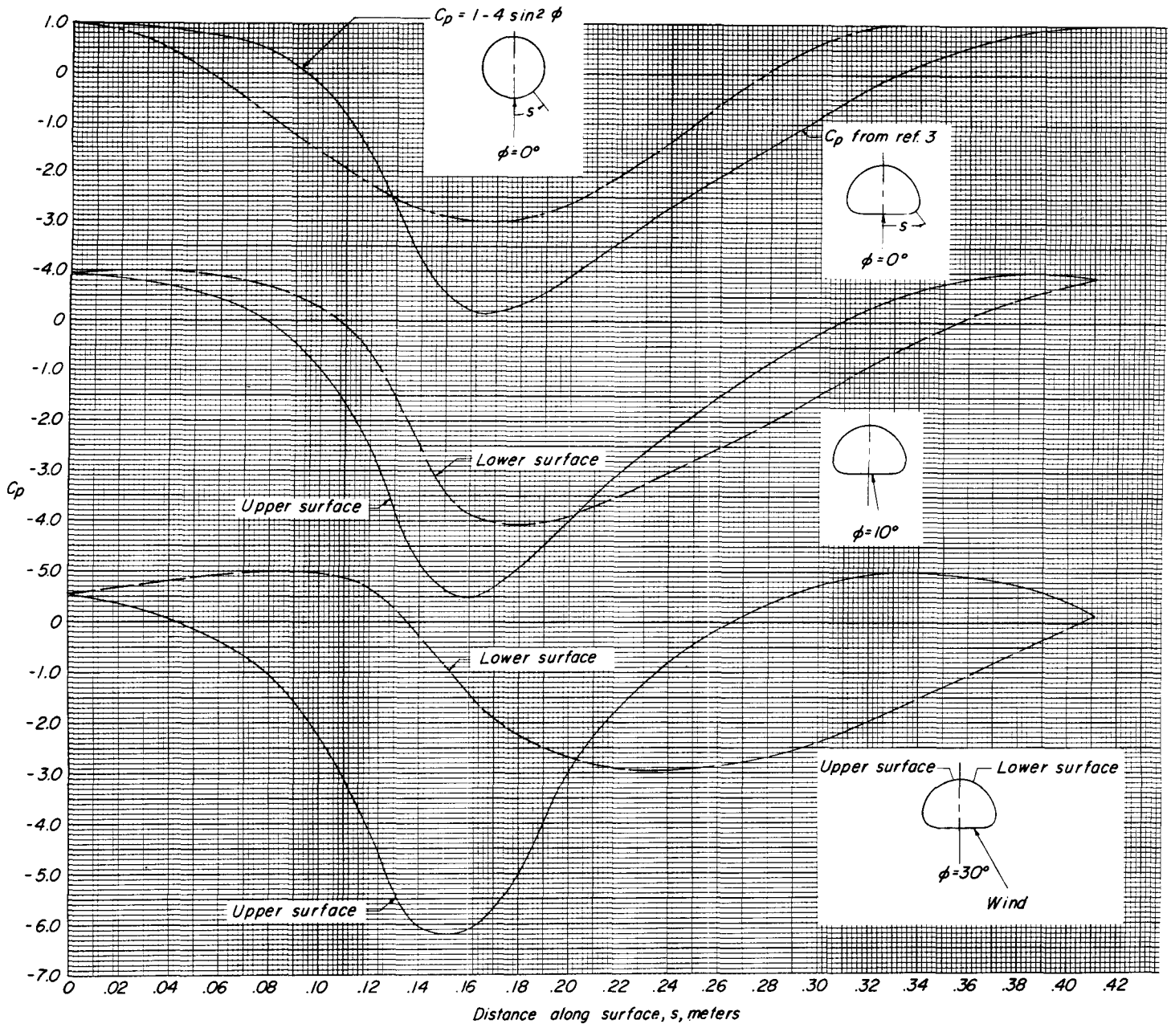

Figure 8.- Theoretical pressure distribution around a circular cylinder and cylinder E of reference 3.

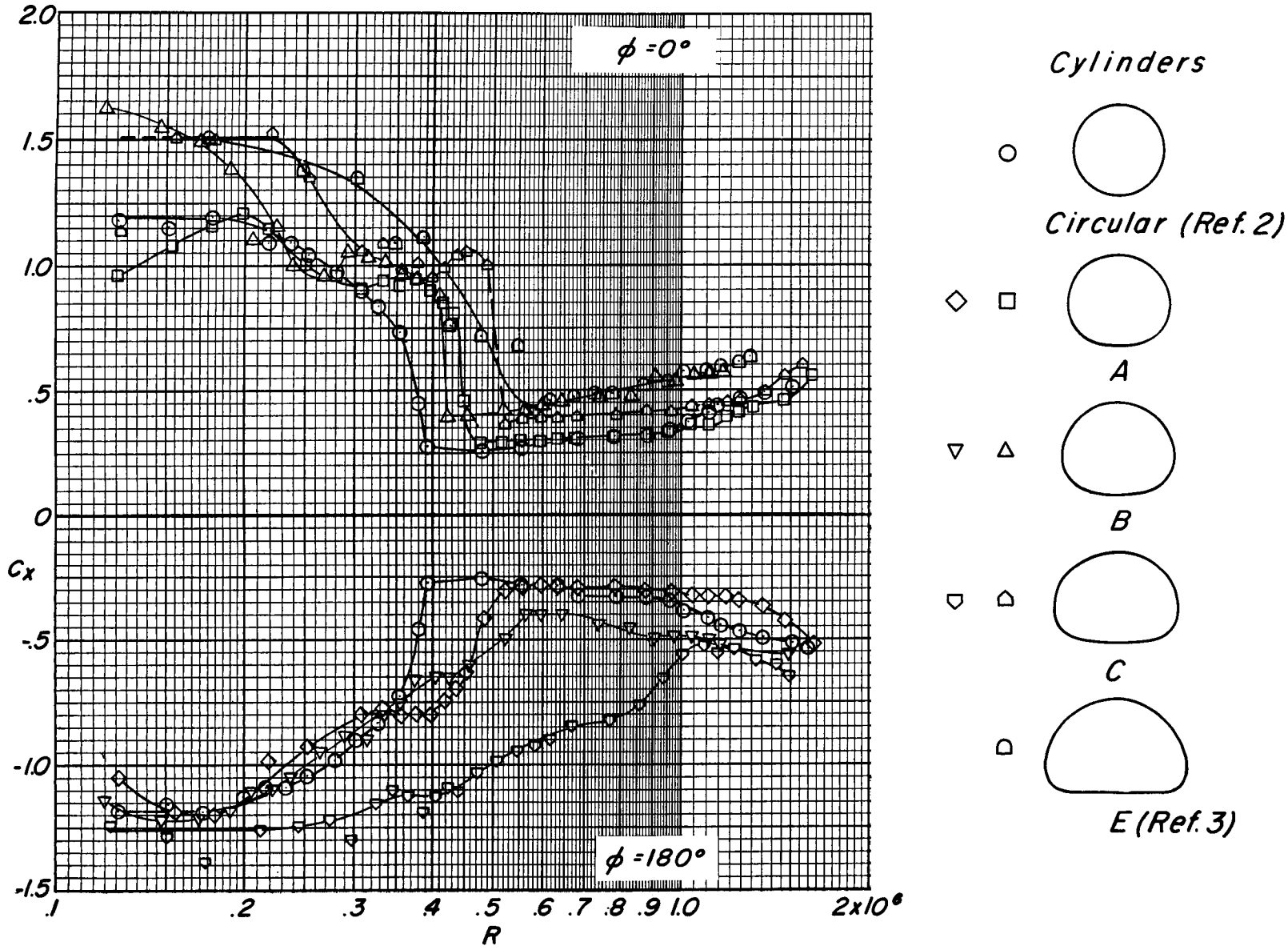

Figure 9.- Comparison of the drag characteristics of various cylinders at $\Phi = 0^0$ and $\Phi = 180^0$.

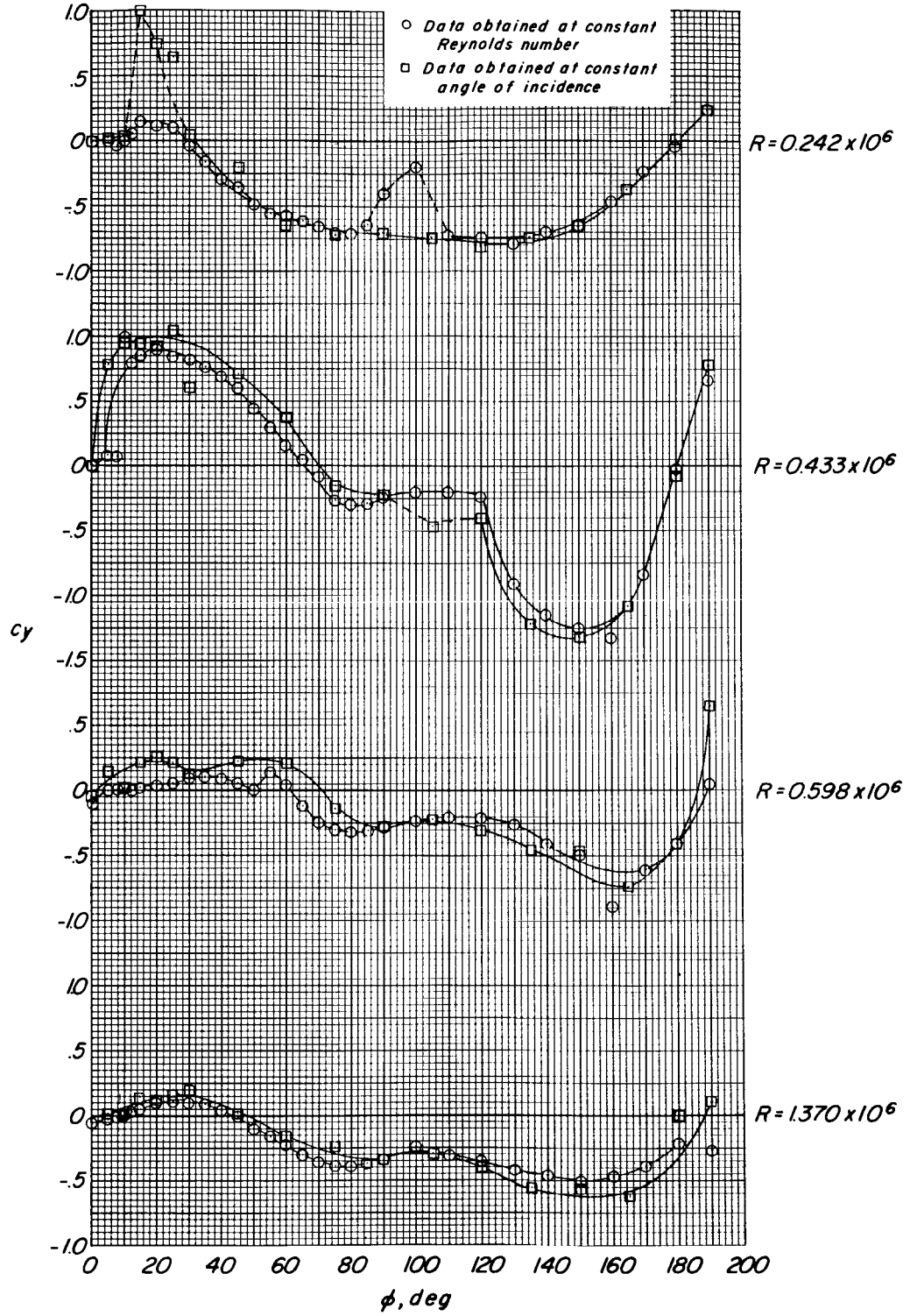

(a) c_y.

Figure 10.- Effect of flow incidence on the force characteristics of cylinder B.

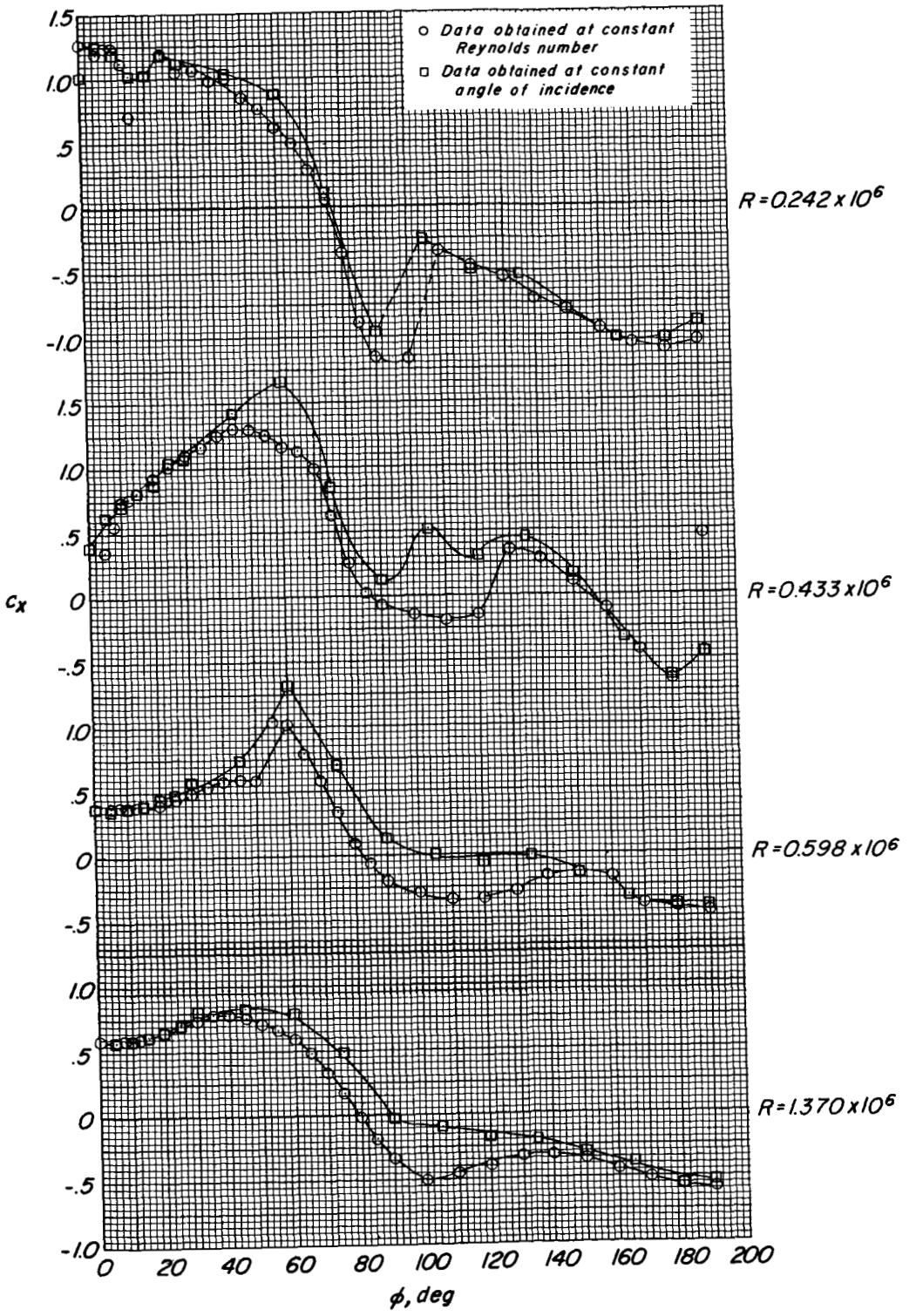

(b) c_X.

Figure 10.- Concluded.

NASA-Langley, 1967 — 13 L-5285

10-5-67

"The aeronautical and space activities of the United States shall be conducted so as to contribute . . . to the expansion of human knowledge of phenomena in the atmosphere and space. The Administration shall provide for the widest practicable and appropriate dissemination of information concerning its activities and the results thereof."

—NATIONAL AERONAUTICS AND SPACE ACT OF 1958

NASA SCIENTIFIC AND TECHNICAL PUBLICATIONS

TECHNICAL REPORTS: Scientific and technical information considered important, complete, and a lasting contribution to existing knowledge.

TECHNICAL NOTES: Information less broad in scope but nevertheless of importance as a contribution to existing knowledge.

TECHNICAL MEMORANDUMS: Information receiving limited distribution because of preliminary data, security classification, or other reasons.

CONTRACTOR REPORTS: Scientific and technical information generated under a NASA contract or grant and considered an important contribution to existing knowledge.

TECHNICAL TRANSLATIONS: Information published in a foreign language considered to merit NASA distribution in English.

SPECIAL PUBLICATIONS: Information derived from or of value to NASA activities. Publications include conference proceedings, monographs, data compilations, handbooks, sourcebooks, and special bibliographies.

TECHNOLOGY UTILIZATION PUBLICATIONS: Information on technology used by NASA that may be of particular interest in commercial and other non-aerospace applications. Publications include Tech Briefs, Technology Utilization Reports and Notes, and Technology Surveys.

Details on the availability of these publications may be obtained from:

SCIENTIFIC AND TECHNICAL INFORMATION DIVISION

NATIONAL AERONAUTICS AND SPACE ADMINISTRATION

Washington, D.C. 20546